The Astrophysical Journal, 671:203–225, 2007 December 10

SCALING RELATIONS OF SPIRAL GALAXIES

Stéphane Courteau
Department of Physics, Engineering Physics and Astronomy, Queen's University, Kingston, ON, Canda; courteau@astro.queensu.ca

Aaron A. Dutton
UCO/Lick Observatory and Department of Astronomy and Astrophysics, University of California, Santa Cruz, CA

Frank C. van den Bosch
Max-Planck-Institut für Astronomie, Königstuhl 17, Heidelberg, Germany

Lauren A. MacArthur
Department of Astronomy, California Institute of Technology, Pasadena, CA

Avishai Dekel
Racah Institute of Physics, Hebrew University, Jerusalem, Israel

Daniel H. McIntosh
University of Massachusetts, Department of Astronomy, Amherst, MA

and

Daniel A. Dale
Department of Physics and Astronomy, University of Wyoming, Laramie, WY
Received 2003 October 15; accepted 2007 July 30

ABSTRACT

We construct a large data set of global structural parameters for 1300 field and cluster spiral galaxies and explore the joint distribution of luminosity L, optical rotation velocity V, and disk size R at I and 2MASS K bands. The I- and K-band velocity-luminosity (VL) relations have log slopes of 0.29 and 0.27, respectively, with $\sigma_{\ln}(VL) \sim 0.13$, and show a small dependence on color and morphological type in the sense that redder, earlier type disk galaxies rotate faster than bluer, later type disk galaxies for most luminosities. The VL relation at I and K bands is independent of surface brightness, size, and light concentration. The log slope of the I- and K-band size-luminosity (RL) relations is a strong function of morphology and varies from 0.25 to 0.5, with a mean of 0.32 for all Hubble types. At most luminosities, early-type disk galaxies have shorter scale lengths than later type ones. The average dispersion $\sigma_{\ln}(RL)$ decreases from 0.33 at I band to 0.29 at K, likely due to the 2MASS selection bias against lower surface brightness galaxies. The VL and RL residuals are largely uncorrelated with each other with a correlation coefficient $r = -0.16$ and $\Delta \log V|L/\Delta \log R|L = -0.07 \pm 0.01$; the $RV - RL$ residuals show a weak positive correlation with $r = 0.53$. These correlations suggest that scatter in luminosity is not a significant source of the scatter in the VL and RL relations. We discuss in two Appendices various pitfalls of standard analytical derivations of galaxy scaling relations, including the Tully-Fisher relation with different slopes. Our galaxy database is available at http://www.astro.queensu.ca/~courteau/data/VRL2007.dat.

Subject headings: dark matter — galaxies: formation — galaxies: kinematics and dynamics — galaxies: spiral — galaxies: structure

Online material: color figures

1. INTRODUCTION

Understanding the origin and nature of galaxy scaling relations is a fundamental quest of any successful theory of galaxy formation. The success of a particular theory will be judged by its ability to predict the slope, scatter, and zero point of any robust galaxy scaling relation at any particular wavelength. Some observed scaling relations in spiral galaxies, based on their size, luminosity, and rotation speed, can be reproduced *individually* to fairly good accuracy by invoking galaxy formation models that include virial equilibrium after dissipational collapse of spherical cold dark matter (CDM) halos and angular momentum conservation (e.g., Mo et al. 1998, hereafter MMW98; van den Bosch 1998, 2000, hereafter collectively vdB; Navarro & Steinmetz 2000, hereafter NS00; Firmani & Avila-Reese 2000, hereafter FAR00; Shen et al. 2002).

One of the most firmly established empirical scaling relations of disk galaxies is the Tully-Fisher relation (TFR; Tully & Fisher 1977), a tight correlation between the total luminosity and the rotation speed of a disk galaxy. We here refer to the TFR as the velocity-luminosity (VL) relation. To date, no single CDM-based model of galaxy formation can *simultaneously* reproduce the slope, zero point, scatter, and color trends of the VL relation, match the shape and normalization of the local luminosity function, and explain the sizes, colors, and metallicity of disk galaxies (see, e.g., vdB; Bell et al. 2003b; Dutton et al. 2007, hereafter D07). In addition, simultaneously accounting for the mass and angular momentum distribution of spiral galaxies in a gas dynamical context remains a major challenge for hierarchical formation models (Navarro & White 1994; van den Bosch et al. 2002; Governato et al. 2007). A complete theory of galaxy scaling relations awaits a fuller understanding of structure forming mechanisms and evolutionary processes (e.g., star formation, merging, feedback, and cooling prescriptions) in galaxies. Likewise, the fine tuning of these galaxy formation and evolutionary models demands a careful examination of empirical scaling relations of galaxies.

In order to set up a framework for the study of galaxy scaling relations, we examine the correlations of parameters related by the virial theorem, $V^2 \propto M/R$. We consider three fundamental observables for each disk galaxy: the total luminosity L, the stellar scale length R_d of the exponential disk, and the observed circular velocity V. The stellar mass, M_*, can be estimated from the luminosity by assuming a stellar mass-to-light ratio, $\Upsilon_* = M_*/L$. The size-luminosity (*RL*) relation of galaxy disks is also expressed as $L \propto \Sigma_0 R_d^2$, where Σ_0 is the disk central surface brightness.

Key to mapping fundamental dynamical trends in spiral galaxies, the measurement of *VL* and *RL* relations and detection of their correlated residuals require velocity amplitudes measured at a suitably chosen radius representative of the flat part of resolved rotation curves, red/infrared magnitudes to minimize extinction and stellar population effects, accurate disk scale lengths, and, ideally, color terms from digital imaging with a broad baseline (e.g., $B-K$) to test for Υ_* variations in the stellar population and extinction effects. One of the goals of this paper is to assemble such a database for field and cluster galaxies (within the limits of available material).

A study of scaling relations in irregular and spiral galaxies by Salpeter & Hoffman (1996) yielded the correlations $L_B \propto R^{2.68} \propto V^{3.73} \propto M_{\rm H\,I}^{1.35} \propto M_{\rm dyn}^{1.16}$, where $M_{\rm H\,I}$, $M_{\rm dyn}$, and R, are the H I and dynamical masses, and a characteristic radius, respectively. The blue luminosities, as used in that study (see also Graham 2002), are notoriously sensitive to dust extinction and stellar population, plus dynamical effects cannot be simply isolated. A new study of scaling relations in the (near-) infrared would provide more robust dynamical constraints to galaxy formation models. While the *VL* relation has been examined at nearly all optical-IR wavelengths (e.g., Strauss & Willick 1995; Verheijen 2001, hereafter V01; Masters et al. 2006; Pizagno et al. 2007, hereafter P07), comparatively few analyses of the *RL* relation of spiral galaxies have been reported so far (Salpeter & Hoffman 1996; de Jong & Lacey 2000, hereafter dJL00; Graham 2002; Shen et al. 2003, hereafter Sh03). This is partly because the accurate disk scale lengths needed to calibrate the *RL* relation, at any wavelength, have only recently become available for large databases (e.g., Courteau 1996; Dale et al. 1999; MacArthur et al. 2003, hereafter MCH03). Furthermore, most investigations of the *VL* and *RL* relations have used grossly incomplete databases owing to the nature of the sample (e.g., single cluster) or selection limits (magnitude, surface brightness, diameter, etc.) The availability of light profiles for very large galaxy databases (e.g., Sloan Digital Sky Survey [SDSS; York et al. 2000] and the Two Micron All-Sky Survey [2MASS; Skrutskie et al. 2006]) heralds a new era for the study of galaxy scaling relations (e.g., Shen et al. 2003; P07) with tractable selection biases.

The empirical *VL* relation is expressed as

$$L \propto V^a, \tag{1}$$

with the near-IR log slope $a \simeq 3.0 \pm 0.2$ (Willick et al. 1997; Giovanelli et al. 1997, hereafter G97; Courteau 1997; hereafter C97; Courteau et al. 2000b; V01; Masters et al. 2006). Reported values of the log slope a range from 2.8 in the blue to 4.0 in the infrared (Willick et al. 1997; Tully & Pierce 2000; V01; P07) for both high and low surface brightness galaxies (Zwaan et al. 1995; V01). However, log slopes steeper than $a \sim 3.5$ in the infrared typically result from small samples and excessive pruning on the basis of idealized morphology or kinematics, a narrow range of inclinations, redshift cutoffs, etc. (Bernstein et al. 1994; V01; Kannappan et al. 2002, hereafter KFF02). The slope, scatter, and zero point of blue *VL* relations are predominantly dominated by stellar population and dust extinction effects (e.g., Aaronson & Mould 1983; G97; Willick et al. 1997; Tully & Pierce 2000; P07) and on the techniques used to recover the major observables and fitting for fundamental relations (e.g., Strauss & Willick 1995; C97; V01; Bell & de Jong 2001; KFF02). Because we are mainly interested in masses, rather than luminosities, we do not concern ourselves with the *VL* and other scaling relations measured at blue wavelengths.

It is shown in Appendix B that previous dynamical derivations of the observed *VL* relation, which arrived at log slopes of 3 (-7.5 in magnitudes) based on the virial relation $M_{\rm vir} \propto V_{\rm vir}^3$ (e.g., MMW98; NS00) and 4 (-10 in magnitudes) based on disk dynamics, used erroneous assumptions. A complete physical interpretation of the *VL* relation is still missing (for a fuller discussion, see, e.g., Gnedin et al. 2006; D07). In terms of observables, the most fundamental relation is between the total *baryonic* mass of a galaxy, inferred via its infrared luminosity, a stellar mass-to-light ratio, and total gas mass (H I+He), and its total mass, inferred from the asymptotic circular velocity of the galaxy disk (McGaugh et al. 2000; Bell & de Jong 2001; V01; McGaugh 2005; Geha et al. 2006; Gurovich 2007; De Rijcke et al. 2007). The "baryonic" *VL* relation is expressed as

$$\mathcal{M}_{\rm bar} \propto V^{a_{\rm bar}}. \tag{2}$$

Since disk gas mass fractions typically increase with decreasing luminosity (e.g., McGaugh & de Blok 1997), one typically has $a_{\rm bar} > a$. The slope $a_{\rm bar}$ is sensitive to the method used to determine stellar mass-to-light ratios. Using stellar populations models, one finds $a_{\rm bar} \simeq 3.5$ (Bell & de Jong 2001; McGaugh 2005), while adopting stellar mass-to-light ratios derived from MOND results in, by construction, $a_{\rm bar} = 4$ (e.g., McGaugh 2005).

While the log slope of the *VL* relation can be reproduced fairly well by naive derivations from CDM-based structure formation models (e.g., MMW98; NS00; D07; see also Appendix B), the predicted scatter can be large compared to the inferred "cosmic" scatter of $\lesssim$0.25 mag in red/infrared bands (Willick et al. 1996; V01; P07) and interpretations about its dependence differ (see below). Besides the basic understanding of the slopes of galaxy scaling relations, the dependence of their scatter has also been addressed by many, especially for the *VL* relation (e.g., Aaronson & Mould 1983; Giraud 1986; Rhee 1996; Willick et al. 1997; KFF02; Courteau et al. 2003), and can be used to set realistic constraints on structure formation models (Courteau & Rix 1999, hereafter CR99; Heavens & Jimenez 1999; FAR00; NS00; V01; Buchalter et al. 2001; Shen et al. 2002; Gnedin et al. 2006; D07). While various trends in the scatter of the blue *VL* relation have been discussed in the past, correlations of the near-infrared *VL* residuals with inclination, size, concentration, gas fraction, or far-infrared luminosity are few and inconclusive (Aaronson & Mould 1983; V01; P07). The dependence of the scatter in the near-IR relation on color and surface brightness is, however, still a matter of contention that we discuss in § 2.3. The scatter in the *RL* relation is also addressed in § 2.3.

The study of scaling relations in galaxies has benefited from the two-pronged application of the *VL* relation for the purposes of (1) Estimating relative distances to measure deviations from the mean Hubble flow (see, e.g., Strauss & Willick 1995 and the reviews in Courteau et al. 2000a), and (2) testing galaxy formation and evolution models (Dalcanton et al. 1997; MMW98; vdB; D07). The philosophy of sample selection and calibration differs in both cases. For cosmic flow analyses, the calibration and science samples must be pruned mainly on the basis of morphology in order to minimize systematic errors and ensure the

TABLE 1
REDSHIFT-DISTANCE GALAXY SURVEYS

Sample (1)	N (2)	Gal. Type (3)	Phot. Bands (4)	Mag./Diam. Limits (5)	Redshift Limits (6)	Rot. Measure (7)
MAT	545	Field	I	$D_{\rm ESO} \geq 1.7'$	$<$7000 km s^{-1}	Hα
SCII	468	Cluster	I	$12 \leq m_I \leq 17$	[5000, 19000]	Hα
Shellflow	252	Field	V, I	$m_B \leq 14.5$	[4500, 7000]	Hα
UMa	38	Cluster	B, R, I, K	$m_z \leq 14.5$	20.7 $\pm$ 0.9 Mpc	H I

smallest possible magnitude (distance) error. Since scatter in the *VL* relation depends strongly on the slope of the relation, it is found that the combination of steepness, magnitude errors, extinction correction, and sky stability favors red (R and I) bands for smallest distance errors and cosmic flows applications (C97; Giovanelli et al. 1997; V01). The accuracy of bulk flow solutions also depends on the size of the sample. In order to collect large enough samples, *VL* calibrations for flow studies rely mostly on H I line widths or Hα rotation curves that can be collected relatively quickly on modest aperture telescopes. These rotation measures based on radio and optical spectra typically sample the disk rotation out to $\sim$3–4 disk scale lengths and are readily calibrated on the same system (C97; Dale et al. 1999).

In contrast, the use of the *VL* relation as a test bed for galaxy formation models requires the widest range of morphological types, to sample all structural properties, and that extinction and stellar population effects be tractable to isolate genuine dynamical correlations. The nearly dust-insensitive infrared bands are thus ideal for such applications (V01). Rotation velocities are preferably extracted from fully resolved H I rotation curves obtained using aperture synthesis maps that sample the disk rotation out to roughly 4–5 disk scale lengths.

Ideally, the study of scaling relations should rely on homogeneous complete volume-limited samples assembled with the very purpose of testing for broad structural and dynamical differences; at the moment, we must contend with the more finely pruned heterogeneous samples of early and mostly late-type spirals that have been collected during the last decade mostly for flow studies. It is currently not possible to correct any of the existing catalogs for incompleteness or assemble a volume-limited sample extending to low mass that is complete in any meaningful sense (e.g., McGaugh 2005). The latest heterogeneous databases, which may include near-infrared luminosities and colors, for large samples of spiral galaxies still enable us to characterize the dependence of scaling relations under the assumption that the different selection biases even out when sufficiently many different samples are collected together and to examine various constraints of structure formation models in ways hitherto unsettled.

Courteau et al. (2003) showed that barred and unbarred galaxies have similar dynamical properties (beyond the corotation radius) and that they share the same *VL* relation. As a natural extension of this study and CR99, we use in §§ 2.2 and 2.3 extensive all-sky distance-redshift catalogs presented in § 2 to characterize the mean *VRL* disk galaxy relations. In an attempt to extend our analysis to the (nearly) dust-free domain, we consider in § 2.4 the infrared photometry from 2MASS for a large sample of spiral galaxies and discuss any relevant caveats. Although 2MASS misses low-luminosity and low surface brightness (LSB) galaxies (McIntosh et al. 2006), it still serves some purposes for our analysis of scaling relations. In § 2.5 we bolster the notion of surface brightness and size independence of the *VL* relation, and we address in § 3 the scatter of the *VL* and *RL* relations and their weak dependence on disk color. The main results are summarized in § 4. The four Appendices give (A) figures for the mean *VRL* relations for each data sample, (B) a derivation on the origin of disk galaxy scaling relations, (C) an alternative derivation of the Tully-Fisher relation, and finally (D) color transformations.

The collected data and basic observations in this paper form the basis of the analytical modeling of spiral galaxy scaling relations in our companion paper (D07). Our basic database is available at http://www.astro.queensu.ca/$\sim$courteau/data/VRL2007.dat.

2. AVAILABLE DATA AND BASIC ANALYSIS

We consider four major samples for which accurate near-infrared galaxy observables and rotational velocities are available. These include (1) the large I-band survey of galaxy distances for bright field spirals in the southern sky by Mathewson et al. (1992; hereafter referred to as the "MAT" survey); the all-sky I-band *VL* surveys of cluster and field spirals by (2) Dale et al. (1999; hereafter referred to as the "SCII" survey), (3) Courteau et al. (2000b; hereafter referred to as the "Shellflow" survey); and (4) the multiband *BRIK VL* survey of Ursa Major cluster galaxies by Tully et al. (1996) and V01 (hereafter referred to as the "UMa" survey). The first three *VL* surveys were originally designed to map the convergence of the velocity field within $\sim$60 h^{-1} Mpc, with the SCII and Shellflow studies paying special attention to *VL* calibration errors for data from different observatories. By design, these surveys favor bright late-type galaxies with inclinations on the sky greater than 45°; most have $i \simeq 60°$.

Properties for each sample are given in Table 1. These include, in column (2), the number of galaxies from the original database that have the full complement of relevant observables; in column (3), the nature of the sampled galaxies (cluster or field; the predominantly "field" MAT and Shellflow surveys include a small fraction of cluster galaxies); and in column (4), the original photometric band coverage. B-band magnitudes for all the MAT galaxies were extracted from the RC3 (de Vaucouleurs et al. 1991). We also have SDSS $g - i$ colors for 39 SCII galaxies (see Appendix C) and *JHK* 2MASS Kron magnitudes and colors for the brightest 360 SCII galaxies; column (5) shows the magnitude or diameter limits of the original catalog; and column (6) shows the redshift limits of the survey in km s^{-1}. For UMa, we adopted the cluster distance of 20.7 Mpc (*HST* Key Project; Sakai et al. 2000); column (7) shows the rotation measure, extracted from spatially resolved H I or Hα rotation curves.

While the MAT and SCII samples used both H I line widths from integrated spectra and Hα rotation velocities from resolved rotation curves, we use only the subsamples of galaxies with available Hα, which is largest for both samples. For the purposes of galaxy structure studies Hα rotation velocities are preferred over H I line widths, as the rotation velocity is measured at a known point of the rotation curve. Furthermore, H I line widths suffer from uncertain turbulence corrections.

Rotation velocities for the Shellflow sample were measured from resolved Hα rotation curves. For the UMa database, we

use the sample of 38 galaxies with $V_{\rm max}$ measured from resolved H I rotation curves (V01).

Disk scale length measurements were computed in somewhat different ways for each sample. For the MAT galaxies, we have used the two-dimensional bulge-disk (B/D) decompositions of MAT *I*-band images by Byun (1992). These decompositions assumed a de Vaucouleurs bulge profile, which is not ideal for late-type galaxies (MCH03), and therefore the extrapolated disk central surface brightnesses may be biased low by a few tenths of a magnitude. Those scale lengths are, however, deemed adequate for the purpose of our study, since they match the mean *RL* relation (see § 2.2). SCII disk scale lengths were obtained by fitting a straight line to the exponential part of the *I*-band surface brightness profile from ~21 to ~25 *I* mag arcsec^{-2} (the so-called marking the disk technique). Shellflow scale lengths were extracted from one-dimensional B/D decompositions of azimuthally averaged *I*-band surface brightness profiles (Courteau et al. 2000b; MCH03). These fits account for a Sérsic bulge and an exponential disk. Disk scale lengths for the UMa sample were measured from a marking the disk technique, but the fit baseline is unspecified, and erratic fits are reported in Tully et al. (1996). The latter could be due to inclusion of bulge light in the disk fit (scale lengths biased low) for the brighter galaxies and sky underestimate (scale lengths biased high) for the fainter galaxies. However, much like MAT, these peculiarities do not affect the UMa *RL* relations as compared against the other samples (see § 2.2 and Appendix A). The conversion of apparent observables to physical parameters uses the distance scale adopted by the original authors, except for UMa galaxies for which we adopted $D = 20.7$ Mpc (Sakai et al. 2000).

Deviations from a smooth Hubble flow may cause distance errors, especially for the nearby galaxies in UMa. For the more distant galaxies in MAT, Shellflow, and SCII, typical thermal velocities of ~200 km s^{-1} would cause relative distance error of ~3%. We find in § 2.1 that distance errors which affect mainly the luminosities and sizes are small compared to the other sources of observational uncertainty. For more details about each sample, the reader is referred to the original papers.

2.1. *Corrections*

In order to homogenize the four data samples, we have applied the inclination corrections for the line widths, luminosities, and scale lengths in a uniform way, as described below.

The rotation velocity estimates are corrected for inclination and redshift broadening using

$$V = V_{\rm obs}/[(\sin i)(1+z)]. \quad (3)$$

The inclination angle is derived via

$$i = \arccos\sqrt{\frac{(b/a)^2 - q_0^2}{1-q_0^2}}, \quad (4)$$

where the semiminor and semimajor axes are determined from CCD isophotal fitting, and q_0 is the intrinsic flattening ratio of edge-on spiral galaxies, here taken to be $q_0 = 0.2$ (e.g., Haynes & Giovanelli 1984; Courteau 1996; Tully et al. 1998; Sakai et al. 2000).

The apparent (*I*-band) magnitudes, m_I, are corrected for both internal extinction, $A_{\rm int}$, and external (i.e., Galactic) extinction, $A_{\rm ext}$. A small *k*-correction, A_k, is also applied such that

$$m_I = m_{I,\rm obs} - A_{\rm int} - A_{\rm ext} - A_k. \quad (5)$$

Internal extinctions are computed using the line width ($W = 2V$) dependent relation from Tully et al. (1998):

$$A_{\rm int} = \gamma_I(W)\log(a/b) = [0.92 + 1.63(\log W - 2.5)]\log(a/b), \quad (6)$$

where a/b is the major-to-minor axis ratio and $\gamma_I(W)$ is a line width dependent extinction parameter. The external (Galactic) extinction is computed using the dust extinction maps of Schlegel et al. (1998), while the *k*-corrections are computed using the line width dependent formalism of Willick et al. (1997).

The absolute magnitudes, *M*, are computed using

$$M = m - 5\log D_L - 25, \quad D_L = \frac{V_{\rm CMB}}{100h}(1+z), \quad (7)$$

where $V_{\rm CMB}$ is the systemic velocity of the galaxy in the reference frame at rest with the cosmic microwave background (Kogut et al. 1993). The *I*- and *K*-band luminosities are computed using for the Sun $M_{I,\odot} = 4.19$ and $M_{K,\odot} = 3.33$.

Disk scale lengths from *I*-band images are corrected for inclination using (Giovanelli et al. 1997)

$$R_I = R_{I,\rm obs}/[1 + 0.4\log(a/b)], \quad (8)$$

and converted into kpc using the distance D_L. The correction above (eq. [8]) is somewhat uncertain, but the choice of observed or deprojected scale lengths does not affect our final results.

Finally, central surface brightnesses are corrected for inclination, Galactic extinction, and cosmological dimming (per unit frequency interval) using

$$\mu_{0,I} = \mu_{0,I,\rm obs} + 0.5\log(a/b) - A_{\rm ext} - 2.5\log(1+z)^3. \quad (9)$$

The coefficient 0.5 in front of the extinction term $\log(a/b)$ is empirically determined by demanding that the residuals of the relation between the *I*-band central surface brightness and rotation velocity has no inclination dependence.[1] We have assumed full transparency in the *K* band. Following Giovanelli et al. (1997), we assume an uncertainty of 15% in γ_I, a/b, $A_{\rm ext}$, and A_k, and propagate the errors. Including distance uncertainties, the average errors on the observables are $\sigma_{\ln V} \simeq 0.09$, $\sigma_{\ln L} \simeq 0.14$, and $\sigma_{\ln R} = 0.15$ (adopting a fitting uncertainty of 15% on disk scale length).

Distance errors in the *VL* relation distance affect mainly luminosity. If we include a distance uncertainty in terms of the recession velocity, the TF scatter is dominated by the uncertainty on *V*, so that linear fits with errors on *V* only or orthogonal fits with errors on both *V* and *L* are almost identical. Distance errors for the *RL* relation can be of issue, since they affect both *R* and *L*. However, since $R \propto D$ and $L \propto D^2$, distance errors move *RL* data points along lines of constant surface brightness. Since the *RL* log slope is ~0.3, the effect of distance errors is minimized. This is especially true given the larger intrinsic scatter and systematic uncertainties in determining scale lengths and correcting for internal extinction.

Hubble types for all but the SCII galaxies were obtained from the heterogeneous NASA Extragalactic Data (NED) base. Most SCII galaxies are not classified in NED, and their morphological types were determined in a homogeneous fashion via a combination of eyeball examination, B/D ratio and/or concentration

[1] For a disk of zero thickness, one expects this factor to range from 0 for an optically thick disk to 2.5 for an optically thin disk.

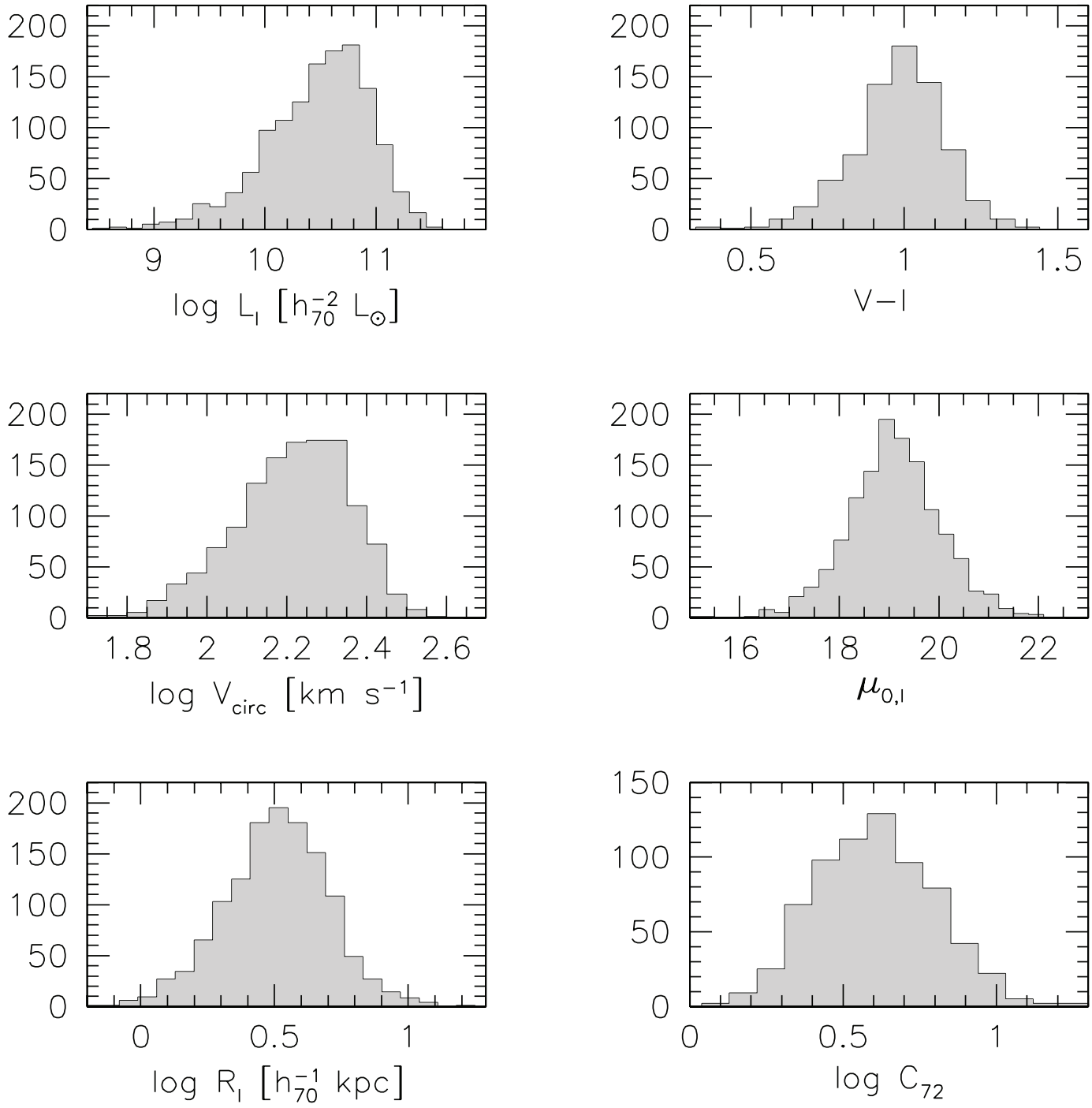

FIG. 1.—Distribution of physical parameters for the four combined data sets.

index (Dale et al. 1999). Interacting and disturbed galaxies were rejected in all samples. In addition to the *VRL* parameters and Hubble types, we have also considered for our study based on optical images the fully corrected $V - I$ color, I-band central surface brightness, $\mu_{0,I}$, and concentration index.

For the Shellflow and UMa samples, $V - I$ and $B - I$ colors were obtained from the original CCD photometry. For the SCII sample, $V - I$ colors were derived from the SDSS (see Appendix C). For the MAT sample, $B - I$ colors were derived from RC3 B magnitudes. We converted $B - I$ colors into $V - I$ colors using the relations between color and stellar mass-to-light ratio in Bell & de Jong (2001). These yielded a total of 742 galaxies with available $V - I$. The central surface brightness $\mu_{0,I}$ are inward extrapolations of the disk fits described above and are available for all galaxies in our compilation.

The galaxy light concentration index can be defined as

$$C_{72} = r_{75}/r_{25}, \tag{10}$$

where the radii enclose 75% and 25% of the total light extrapolated to infinity. For reference, a pure exponential disk has $C_{72} = 2.8$, regardless of its total mass or scale length. Concentration indices for the MAT sample were not available. In total, 691 galaxies in our compilation have C_{72} estimates.

Altogether, the MAT, SCII, Shellflow, and UMa samples combine for a total of 1303 separate entries. The range of physical

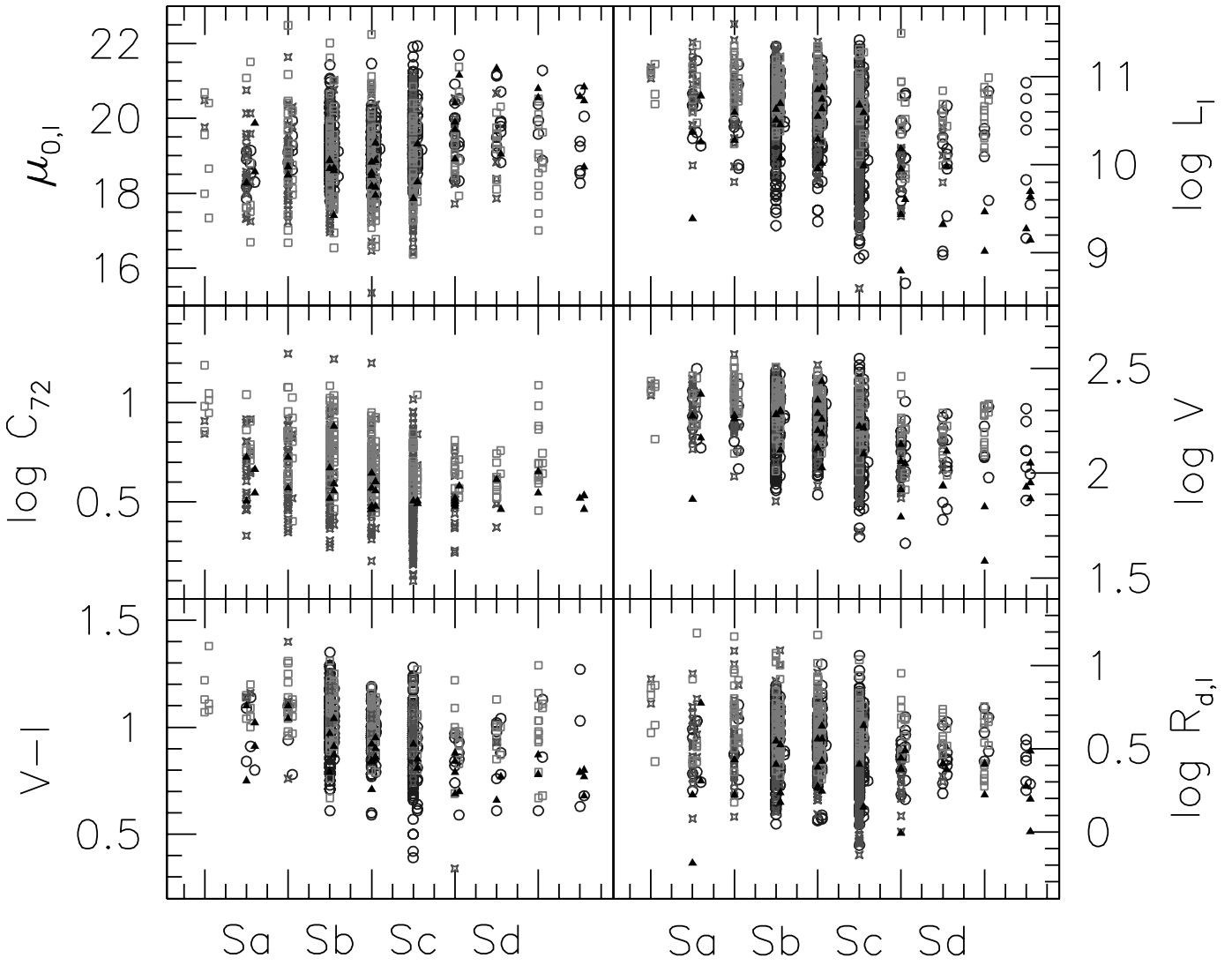

FIG. 2.—Correlation of galaxy observables (disk central surface brightness [$\mu_0 \equiv -2.5 \log I_0$], concentration C_{72}, $V - I$ color, luminosity L_I, rotation speed V, and disk scale length $R_{d,I}$) with morphological type. The point types represent each sample: *blue squares*, Shellflow; *red stars*, SCII; *green circles*, MAT; and *black triangles*, UMa. There is a weak dependence of all variables on Hubble type, with an apparent flattening of the trends for Sc galaxies and later. [*See the electronic edition of the Journal for a color version of this figure.*]

parameters for our combined data set is shown in Figure 1. This range is broad in every respect, yet not complete in any statistical sense. We have not endeavored to correct each sample for incompleteness due to the complex inherent selection biases. Most parameter distributions can be closely approximated by a lognormal function. The relations between morphological type and luminosity, rotation velocity, size, color, surface brightness and concentration are shown in Figure 2. The distributions for all the parameters except $\mu_{0,I}$ are broadly similar, with a gentle decline from the highest mean values for the earliest type systems (Sa) down to intermediate types (Sbc), settling onto a constant mean level for types Sc and later. This global trend is roughly reversed for $\mu_{0,I}$. Our study of galaxy scaling relations will be extended to the K-band based on 2MASS data in § 2.4 for comparison purposes.

2.2. *Mean Parameter Relations*

We consider the joint projected distribution in each of the planes defined by a pair of the three log virial variables, log R_d, log V, and log L_I for the four combined samples in Figure 3; the distributions for the individual SCII, MAT, Shellflow, and UMa samples are shown in Appendix A. Different symbols identify the full range of spiral Hubble types.

The fits shown as solid black lines in each *VRL* figure are the orthogonal linear fits to the full combined data sets of 1303 galaxies. Table 2 gives the results of the orthogonal fits using propagated errors on both variables (see e.g., Akritas & Bershady 1996) for the full sample and for each Hubble type; the errors on the slopes and zero points correspond to 1 σ deviations assessed by bootstrap resampling. The regressions were performed over the full available range of luminosities, sizes, and velocities. The number of galaxies per Hubble type is shown in parentheses. The need for more measurements of the earliest and latest type spirals is obvious.

We choose orthogonal fits over forward, inverse, or bisector fits for the following reasons. Forward and inverse fits make the assumption that scatter exists *only* in the dependent variable. Since it is not possible for both forward and inverse fits to be correct, bisector fits, which average the forward and inverse fits, can also not be correct (indeed, the bisector fit of a perfectly uncorrelated distribution of two variables has an absolute slope of one). Furthermore,

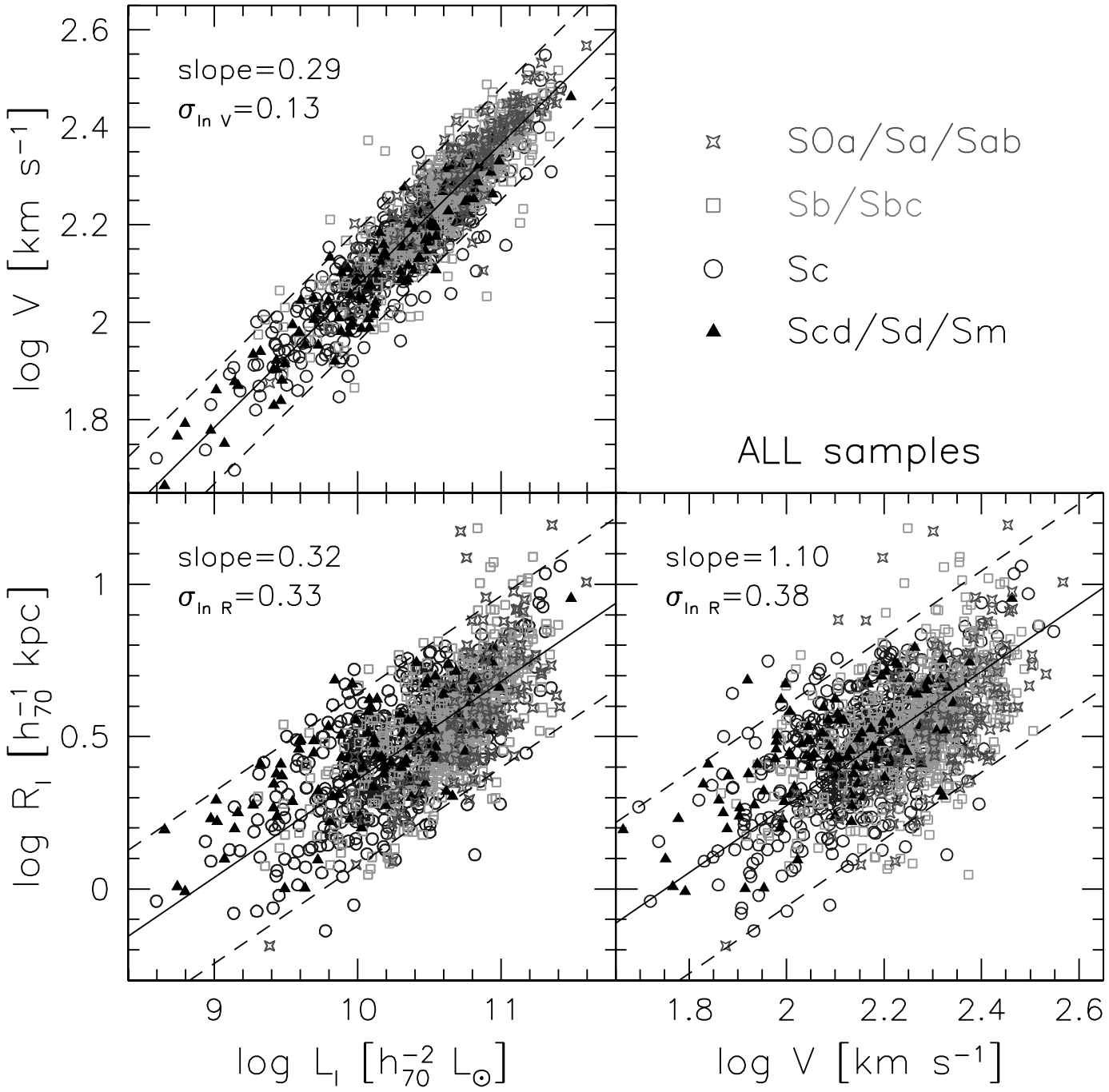

FIG. 3.—*VRL* scaling relations for all four samples color-coded by Hubble types. The linear orthogonal fits, shown by the solid lines, are reported in Table 2 for the combined samples; the 2 σ observed scatter are given by the dashed lines. [*See the electronic edition of the Journal for a color version of this figure.*]

unlike orthogonal fits, forward and inverse fits cannot account for measurement uncertainties on both variables simultaneously.

The combined *I*-band data give a *VL* relation, $V \propto L^{\alpha}$, with log slope $\alpha_I = 0.29 \pm 0.01$. The agreement between the log slopes for the *VL* relations for different samples, as judged from Figures 14–17 in Appendix A is fairly good. Our *VL* fit is also a close match to those published by the original authors (as $M_I \propto \log V$), even though the minimization techniques can be quite different. The Pearson correlation coefficient of the *VL* relation is $r = 0.92$, and the conditional distribution of $V|L$ is roughly lognormal. Our *VL* relation, which uses optical rotational velocities, is a close match to the *I*-band *VL* relation of Masters et al. (2006) for their SFI^{++} catalog of 807 cluster galaxies when allowance is made for line width differences.[2]

The correlations for the *RL* and size-velocity (*RV*) relations are weaker, averaging $r \sim 0.65$. The *RL* relation for the full sample, $R \propto L^{\alpha}$, has a log slope $\beta_I = 0.32 \pm 0.01$. Since the fits of the *VL* and *RL* relations are more robust than the *RV* relation, we adopt

[2] The *I*-band *VL* relation of Masters et al. (2006) is based on H I line widths and normalized to Sc galaxies. Application of their transformation from Hα to H I (see their eq. [2]) results in a steeper slope for the *VL* relation based on H I line widths. This explains in part the difference between the shallower log slope of our *VL* relation (0.29) and theirs (0.32).

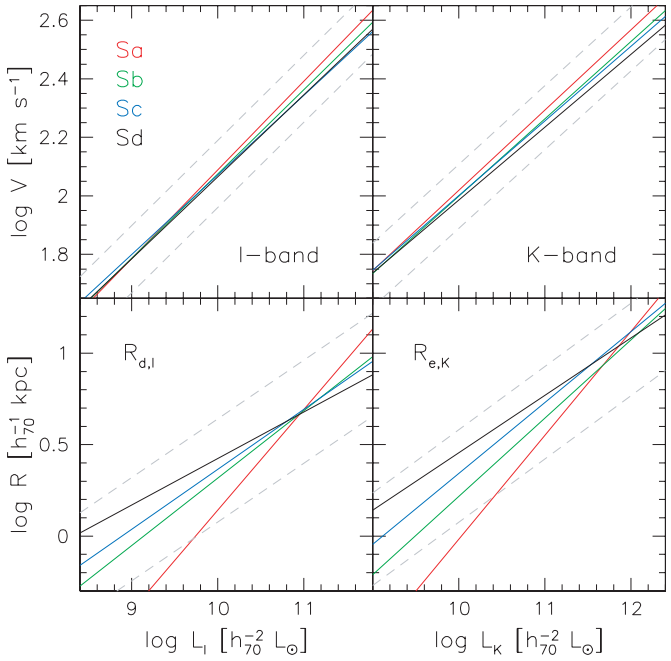

FIG. 4.—*VL* and *RL* relations color-coded by Hubble types: combined *I*-band sample (*left*), SCII *K*-band sample (*right*; the latter is discussed in § 2.4). The gray dashed lines show the 2 σ scatter of the *VL* and *RL* relations for the full *I*- and *K*-band samples. At *I* band, $R = R_d$, the disk scale length; at *K* band, we used $R = R_e$, the effective radius of the galaxy supplied by 2MASS. The *VL* relation shows, on average, that earlier type spirals rotate faster than later types at a given luminosity. The *RL* relation depends strongly on morphology with earlier types showing a steeper (∼constant surface brightness) slope.

an *RV* relation requiring self-consistency between the three relations. That is, if $V \propto L^{\alpha}$ and $R \propto L^{\beta}$ and $R \propto V^{\gamma}$, then $\gamma = \beta/\alpha$.

Size-dependent distributions are less robust than the *VL* relation, owing to such factors as (1) a lack of a uniform and universal definition of scale length (MCH03), (2) a morphological dependence that we discuss in § 2.3, (3) a larger intrinsic scatter due to the natural dispersion of the spin parameter λ (D07), and (4) a susceptibility to surface brightness selection effects. Whether scale lengths are measured from B/D decompositions or "marked" over a specified range of surface brightnesses (while omitting the bulge region or not) can yield scale differences greater than 20% (MCH03). Again, the overlap between the four samples is too small to assess systematic errors. It is therefore difficult to determine how much of the lower correlation coefficients in the *RL* and *RV* relations is genuine and/or due to inadequate scale lengths.[3] Despite potential pathologies with the MAT scale lengths (see § 2), the scaling relation slopes for this sample and SCII are comfortably close. In spite of intrinsic differences between each sample (especially selection functions), we make the assumption that our calibration in § 2.1 brought all the samples on the same system.

It has been proposed that the scaling relations may be different for the fainter, LSB galaxies (e.g., Kauffmann et al. 2003; Shen et al. 2003), where gas fractions are likely to be different. Such a departure is not apparent in the samples that most closely probe the LSB regime (SCII and MAT; see Figs. 14 and 15 in Appendix A). Our observations are also corroborated by the study of low-mass dwarf galaxies of Geha et al. (2006), who finds no break in the TF relations of very faint and brighter spiral galaxies.

In summary, we find that the mean *I*-band scaling relations for spiral galaxies in Table 2 are

$$V \propto L_I^{0.29}, \quad R_d \propto L_I^{0.32}, \quad R_d \propto V^{1.10}. \tag{11}$$

The uncertainties in the log slopes for the SCII sample, which we use as our baseline, are ±0.01 (*VL*), ±0.02 (*RL*), and ±0.12 (*RV*) based on 1 σ measurement errors.

A study of the volume-corrected *RL* distribution for 140,000 late-type SDSS spirals (Sh03) has yielded log slopes from $\beta = 0.23$ (low *L*) to $\beta = 0.53$ (high *L*), with scatter ranging from $\sigma_{\ln R} = 0.45$ (low *L*) to 0.30 (high *L*). These results are fully consistent with ours; see Table 2, where our *I*-band *RL* log slopes agree perfectly with those of Sh03. This nearly perfect agreement must be contrasted in light of various caveats, including the fact that the size measurement in Sh03 uses the Sérsic half-light radius, fit to a circularized SB profile. The median half-light radius of their sample is 2″, compared to a mean seeing FWHM of 1.5″, which is cause for concern. The morphological sampling of the SDSS study also differs significantly from that of our collected samples. The size measurements are thus different from ours and possibly called into question due to seeing contamination and poorly matched profile shapes (see e.g., MCH03).

The MAT sample (see Fig. 15, below) was also analyzed by dJL00, who attempted to correct for statistical incompleteness; they found the range $\beta = 0.2$–0.3. Our (noncorrected) result for the MAT sample alone is $\beta = 0.28 \pm 0.01$ consistent with the upper envelope of dJL00. The completeness correction affects mostly the low *L* distribution. At a given luminosity, one magnitude of surface brightness corresponds to 0.2 dex in R_d, and a (complete) population of LSB galaxies would give a shallower log slope in agreement with dJL00. The effect is subtle, given the large intrinsic size errors, but we must keep that caveat in mind.

2.3. *The Morphological/Color Dependence of Galaxy Scaling Relations*

A simple understanding of the morphological dependence of the *VL* and *RL* relations is provided by Figure 4. We detect a slight

[3] The improved reliability of scale length measurements must come from an extensive program of deep near-infrared imaging to measure homogeneous and accurate disk scale lengths and half-light radii for a very large collection of spiral galaxies based on a single reduction method and high signal-to-noise data.

TABLE 2
ORTHOGONAL FITS FOR THE FOUR COMBINED *I*-BAND SAMPLES

		log *V* vs. log L_I			log $R_{d,I}$ vs. log L_I		
TYPE	*N*	Slope	Zero Point	$\sigma_{\ln V\|L}$	Slope	Zero Point	$\sigma_{\ln R\|L}$
All	1303	0.291 ± 0.004	−0.835 ± 0.039	0.132	0.321 ± 0.010	−2.851 ± 0.106	0.325
V − *I*	742	0.297 ± 0.005	−0.898 ± 0.056	0.131	0.306 ± 0.013	−2.681 ± 0.136	0.304
Sa	117	0.303 ± 0.013	−0.941 ± 0.140	0.126	0.550 ± 0.047	−5.357 ± 0.501	0.375
Sb	570	0.288 ± 0.008	−0.805 ± 0.084	0.132	0.369 ± 0.020	−3.373 ± 0.213	0.313
Sc	505	0.272 ± 0.006	−0.648 ± 0.060	0.126	0.328 ± 0.015	−2.915 ± 0.156	0.320
Sd	111	0.280 ± 0.011	−0.735 ± 0.111	0.125	0.254 ± 0.021	−2.116 ± 0.213	0.289

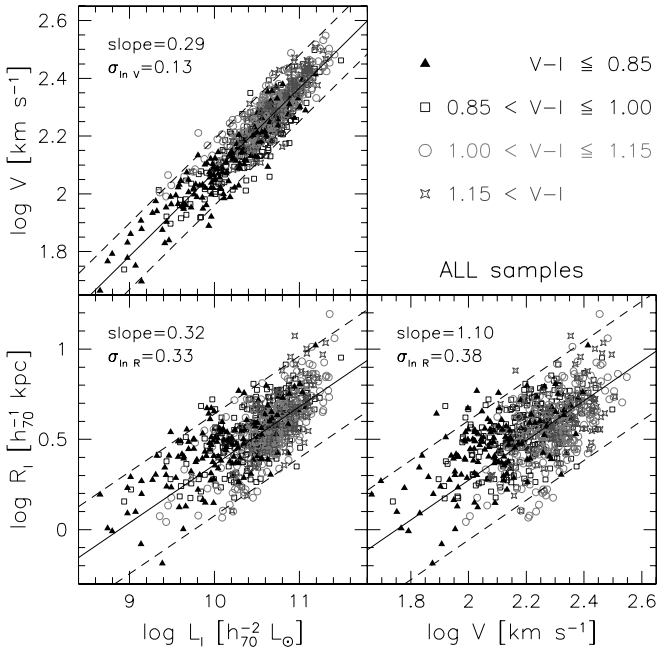

FIG. 5.—Same as Fig. 4, but with point types representing different $V - I$ color. The *VL* relation shows a weak dependence on color. [*See the electronic edition of the Journal for a color version of this figure.*]

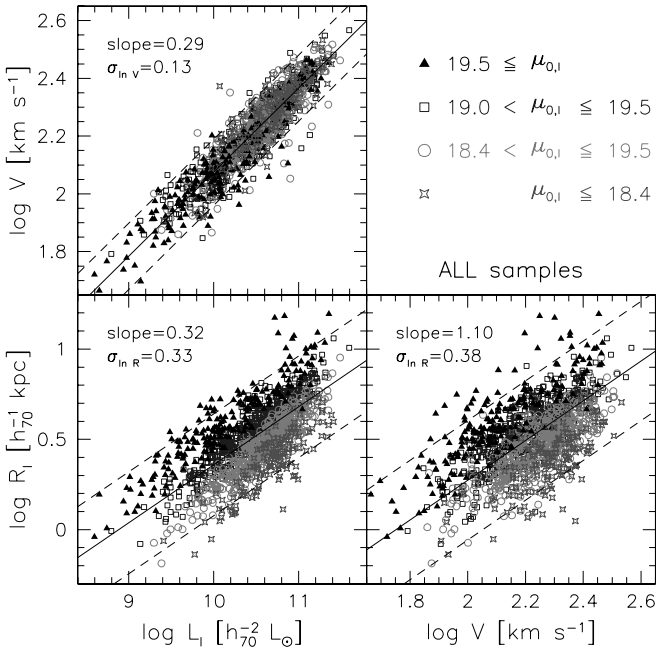

FIG. 6.—Same as Fig. 4, but with point types representing different central surface brightness. The *VL* relation is fully independent of surface brightness, whereas the *RL* relation shows the trivial dependence on surface brightness. [*See the electronic edition of the Journal for a color version of this figure.*]

and a strong morphological dependence of the *VL* and *RL* relations, respectively. This is confirmed by examination of Table 2. The morphological dependence of the *VL* relation was first discussed by Roberts (1978) and revisited by Aaronson & Mould (1983), Rubin et al. (1985), Giraud (1986), Pierce & Tully (1988), G97, and KFF02, to name a few. It goes in the sense of early-type spirals rotating faster than later ones at most optical luminosities. The strong morphological dependence of the *RL* relation is such that earlier type spirals are more compact than the later ones at most low to intermediate luminosities. This trend is reversed for the brighter galaxies with $L \geq 10^{11}\ L_\odot$. For early-type (Sa) galaxies, the *RL* log slope is close to the nominal limit of 0.5 for constant surface brightness (since $\Sigma_0 \propto L/R_d^2$). The *RL* log slopes are progressively shallower from early- to late-type systems.

We can refer to Figure 2 to assess whether a correlation with morphological type is driven by any other galaxy parameters. On the basis of smallest scatter, the strongest correlations with morphological type would be with color (see also Roberts & Haynes 1994; Fig. 5) and velocity. Given that color is linked to the mean stellar M/L ratio and star formation history (SFH) of the galaxy (Bell & de Jong 2001; Bell et al. 2003b; Portinari et al. 2004), the latter might thus be a source of scatter in the *VL* relation (e.g., Heavens & Jimenez 1999; D07). One expects the *VL* scatter in bluer bands to be more sensitive to contributions of instantaneous star formation activity, while at (near-) infrared bands the scatter from stellar population effects mainly reflects the convolved star formation histories.

The analysis of the Nearby Field Galaxy Survey (Jansen et al. 2000) by KFF02 identified $B - R$ color and Hα equivalent width as the main drivers of the scatter in the optical *VL* relation. Color and Hα equivalent width are both tributary of star formation histories, although the former depends both on the *integrated* and instantaneous star formation, while the latter is a function of the current star formation rate alone. We do detect a weak color dependence of the *I*-band *VL* relation (Fig. 5; see also Fig. 7, below). This result is further confirmed in § 3 and Figure 13, below, and independently by P07. The trends are such that redder disks rotate faster and are more compact than bluer ones. However, while color may contribute to the *VL* scatter, we shall conclude in § 3 that it is not a dominant source of scatter to either the *VL* or *RL* relations.

Other than observational errors and scatter in luminosity due to variations in the SFH, *VL* scatter is also expected from variations in the halo concentration parameter and, to a lesser extent, scatter in the galaxy spin parameter and disk mass fraction. A discussion of the relative contributions to the *VL* scatter from SFH and halo parameters is presented in D07.

According to V01, all correlations of *VL* residuals with galaxy observables detected in blue bands, including color, which affects the zero point, vanish in the infrared. This important assertion, however, rests on the study of a small data sample and deserves closer attention. Contrary to findings by Aaronson & Mould (1983) and V01, Rubin et al. (1985) found that the morphological type dependence of the *VL* relation was reduced, but not eliminated, at infrared *H* luminosities. In § 2.4, we make similar tests for any variations of the *VL* and *RL* relations at infrared wavelengths.

2.4. *Surface Brightness Independence of the VL Relation*

Previous reports of the correlation of *VL* residuals with disk surface brightness may have generated confusion. Willick (1999) reported a correlation of *I*-band *VL* residuals with surface brightness and compactness for his "LP10K" survey of distant cluster galaxies using a moments fitting method to determine the exponential disk parameters even in the presence of irregularities in the galaxy light profiles. In an attempt to alleviate subjective fitting boundaries, Willick's method used the entire surface brightness profile, including the bulge, thereby biasing the scale length and central surface brightness measurements. Applying his procedure, we can reproduce the putative surface brightness dependence of the *VL* relation, while proper bulge-to-disk (B/D) fitting techniques (MCH03) find none.

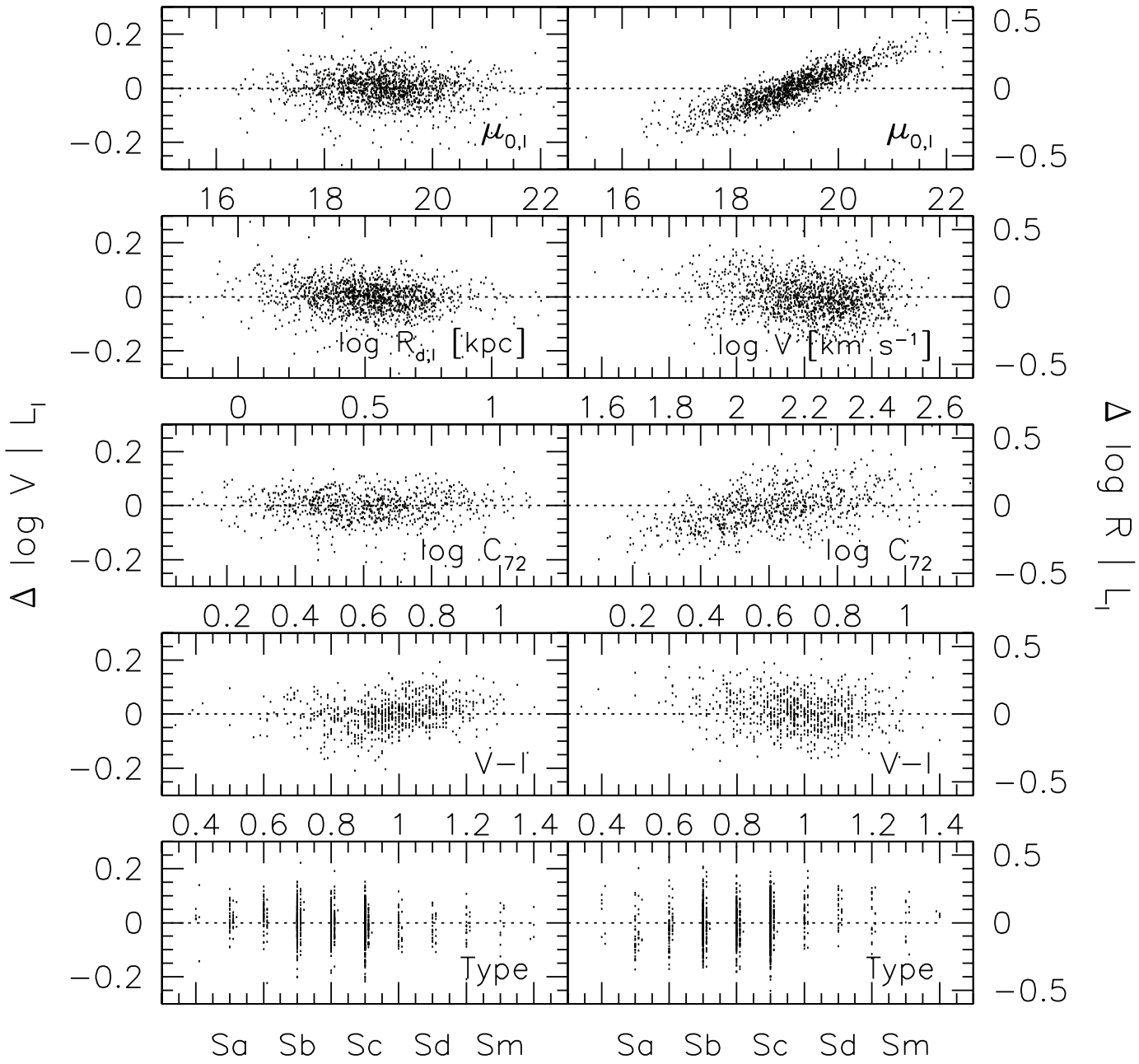

FIG. 7.—Residuals from the *VL* (*left*) and *RL* (*right*) relations as a function of disk central surface brightness, disk scale length, rotation velocity, concentration index, $V - I$ color, and optical morphological type for all the galaxies in our sample. Besides the expected dependence of the *RL* relation on μ_0, the scatters of the *VL* and *RL* relations may show weak correlations on color and concentration, respectively.

Prior to this study, the absence of surface brightness dependence of the *VL* relation had also been verified at optical bands by Sprayberry et al. (1995), Zwaan et al. (1995), and CR99, and in the infrared by V01. Our Figures 6 and 7 (see also Figs. 10, and 11, below) corroborate this evidence very clearly; namely that there is no dependence of the *VL* relation scatter on *I*-band central surface brightness $\mu_{0,I}$ or *K*-band effective surface brightness.

The surface brightness independence of the *VL* has been interpreted (e.g., Zwaan et al. 1995) as variation of the dynamical mass-to-light ratio, $\tilde{\Upsilon}$, with surface brightness for a given total luminosity. If the surface brightness decreases, $\tilde{\Upsilon}$ increases in such a way that the *VL* relation remains independent of surface brightness. A dependence of $\tilde{\Upsilon}$ on surface brightness is indeed expected in CDM-based galaxy structure models; the higher the disk surface brightness, the higher the contribution of baryons to the rotation velocity at, say, 2.2 disk scale lengths (Zavala et al. 2003; P05; D07). However, reproducing the surface brightness independence of the *VL* relation is a nontrivial task, especially for the highest surface brightness galaxies (CR99; D07). Indeed, for a given disk mass and dark halo profile, a small disk (higher surface brightness) would contribute significantly to $V_{2.2}$, the total circular velocity at 2.2 disk scale lengths.[4] In the absence of halo contraction, the contribution of the halo to $V_{2.2}$, for typical halo concentrations, slightly decreases as disk size decreases. The net effect is typically that $V_{2.2}$ increases as disk size decreases (CR99; D07). When halo contraction is included a smaller

[4] The maximum velocity measurements collected in our database correspond roughly to $V_{2.2}$.

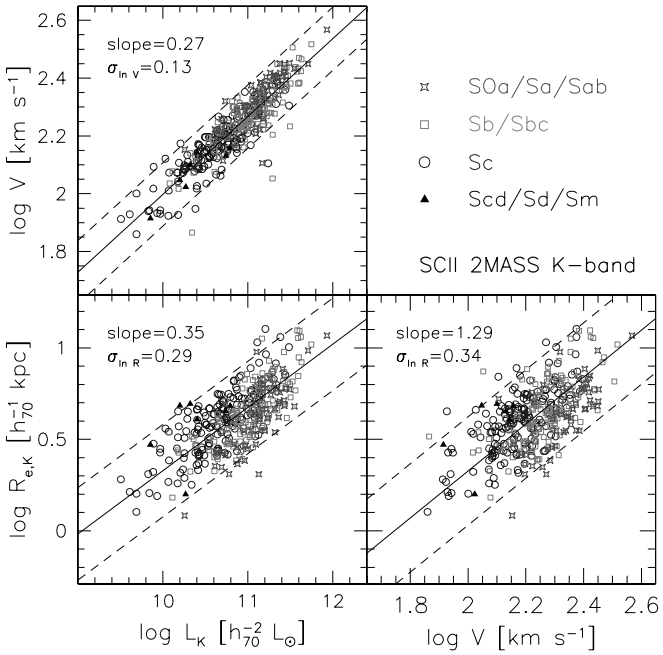

FIG. 8.—*VRL* scaling relations of the SCII *K*-band sample separated by Hubble types. The linear orthogonal fits, shown by the solid lines, are reported in Table 3 for the combined samples; the 2 σ observed scatter are given by the dashed lines. [*See the electronic edition of the Journal for a color version of this figure*.]

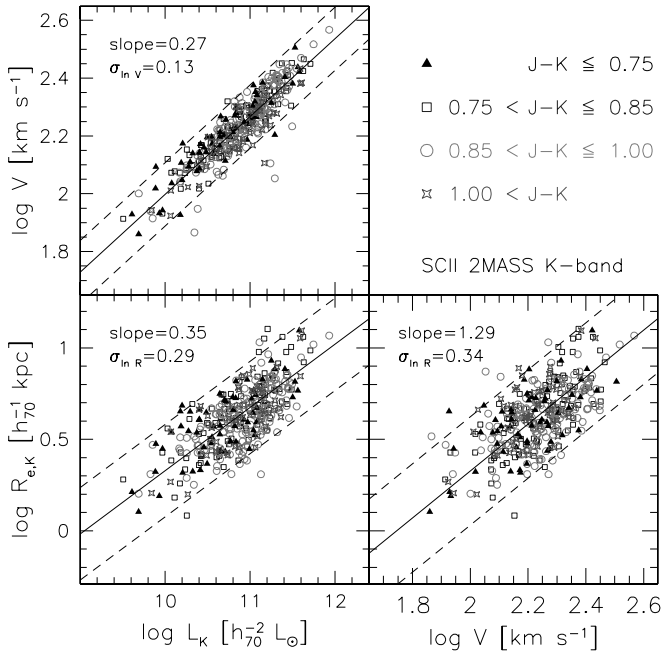

FIG. 9.—Same as Fig. 8, but with point types representing different $J - K$ colors. The *VL* relation shows a weak dependence on color, while the *RL* and *RV* relations show none. [*See the electronic edition of the Journal for a color version of this figure*.]

disk results in a smaller halo and hence even higher total $V_{2.2}$ (D07).

Gnedin et al. (2006) circumvent this problem by assuming that at a given stellar mass, smaller and thus higher surface density disks live in less massive halos. This solution is not particularly attractive as it has neither observational nor theoretical motivation. On the other hand, the observed dependence of gas-to-stellar mass ratio on surface brightness is effective in reducing the surface brightness dependence of the *VL* relation (FAR00; van den Bosch 2000; D07). Furthermore, if galaxy formation involves clumpy cold flows, rather than smooth cooling flows, dynamical friction between the baryons and dark matter may reverse some (or all) of the expected effects of halo contraction, thus reducing the surface brightness dependence of the *VL* relation (D07).

2.5. *The Infrared* (*2MASS*) *Velocity-Luminosity and Size-Luminosity Relations*

The advent of large-scale infrared surveys, such as 2MASS, provides us with *JHK* luminosities, effective (i.e., half-light) radii, and near-infrared colors to construct (nearly) dust-free scaling relations. However, with a typical surface brightness limit of $K \sim 20$ mag arcsec^{-2}, the 2MASS luminosity profiles are a full 2 mag shallower than the typical *I*-band surface brightness profiles for our galaxies. Still, the 2MASS data yield scaling relations that are as tight as the ones derived at *I* band, with log slopes representative of higher surface brightness systems. So while 2MASS data may be ill-suited for deep imaging investigations of galaxies (see e.g., Bell et al. 2003b) and deriving the correct slopes of the *VL* and *RL* relations (see, however, Kudrya et al. 2003), the information that they provide about the scatter of (2MASS) IR scaling relations may still be useful. Because of the 2MASS magnitude limit of 13.5 *K* mag, only the 360 brightest SCII galaxies have measured 2MASS magnitudes. For simplicity, our analysis of *K*-band scaling relations is restricted to the SCII sample. Note also that we make use of effective radii, supplied in the 2MASS data pipeline, rather than disk scale lengths for this sample. For reference, a pure exponential disk has $R_e = 1.678R_d$.

We correct the IR data in a manner analogous to the optical data in § 2.1. We use the *K*-band correction from Tully et al. (1998) scaled using the standard Galactic extinction curve (Schlegel et al. 1998) to get *JHK* extinctions. These corrections remove any inclination dependences on the *VL* and color-*L* relations. We do not find any evidence of an inclination dependence to the values of $R_{e,K}$ and $\mu_{e,K}$ and thus no corrections to these quantities were applied.

Figures 8, 9, and 10 show the *K*-band *VRL* relations for the 360 brightest SCII galaxies, as reported in Table 3. Based on this sample, the 2MASS infrared scaling relations are $V \propto L_K^{0.27}$, $R_{e,K} \propto L_K^{0.35}$ and $R_{e,K} \propto V^{1.29}$. Thus, the *I*-band and 2MASS *K* band for the bright SCII sample have comparable *VL* relations, but the log slopes for the *RL* and *RV* relations differ substantially. We must keep in mind that the 2MASS *RL* and *RV* log slopes are biased against the lower surface brightness SCII galaxies, and hence the steeper log slopes for the *RL* and *RV* compared to the *I* band. If we restrict the *I*-band sample of SCII galaxies to the bright 2MASS subsample, we find nearly identical *I*-band log slopes for the *VL* (0.28) and R_eL (0.36) relations. This confirms that the different slopes for the *I*- and *K*-band *RL* relations result purely from selection, rather than a systematic difference between the *I*-band disk scale lengths and *K*-band effective radii, or putative pathologies with the 2MASS sizes.

Because the *VL* relation is surface brightness independent, which we verify for 2MASS data in Figure 10, we can still use these data to assess the parameter dependence in the *VL* and, to a lesser extent, the (incomplete) *RL* relation.[5]

[5] Although 2MASS surface brightness profiles only reach $K \sim 20$ mag arcsec^{-2}, the 2MASS $J - K$ color terms are still useful for the separation of redder and bluer disks since IR galaxy bulge and disk color gradients are already substantial after one disk scale length (MacArthur et al. 2004).

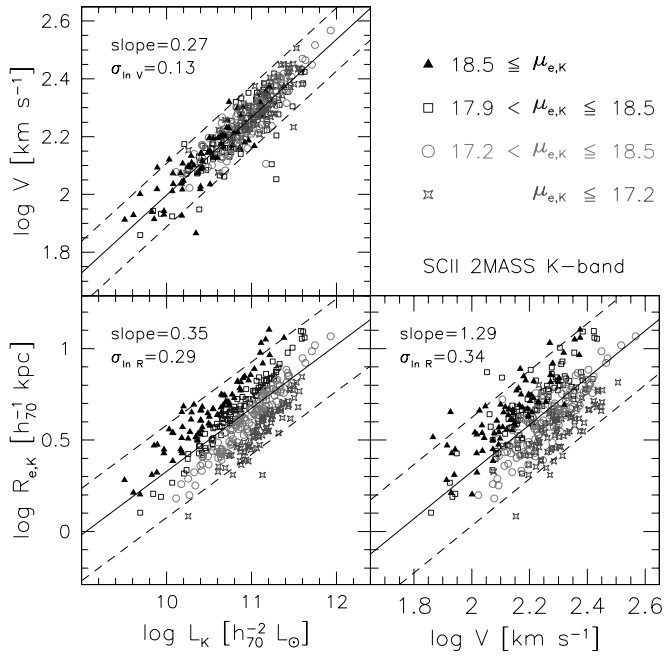

FIG. 10.—Same as Fig. 8, but with point types representing different effective surface brightnesses. The *VL* relation is independent of surface brightness, while the *RL* relation shows a trivial dependence on surface brightness. [*See the electronic edition of the Journal for a color version of this figure.*]

The *K*-band *VL* and *RL* relations show similar dependences on morphological type as the *I*-band relations (Fig. 4). As we see from Figures 8–11 the slope, zero point, and scatter of the *K*-band *VL* relation is fully independent of surface brightness, size, and concentration parameters. Any correlation with color, $J-K$ this time, is difficult to assess given the paucity of late-type systems in this sample; the $V-I$ color dependence that was more prominent (although barely) in Figure 7 seems to have vanished at NIR wavelengths in Figure 11. The *RL* relation shows the usual dependence on surface brightness and no dependence on $J-K$ color.

3. RESIDUAL CORRELATIONS OF SCALING RELATIONS

In the spirit of CR99, we now examine below the correlations of the *VL*, *RL*, and *RV* residuals from the mean relations. We define the residuals for each object i as $\Delta y(i) \equiv y(i) - y_{\rm fit}(i)$. The orthogonal fits for the global scaling relations on *VRL* were described in § 2.2.

Figure 12 shows the residual correlations for combinations of $\Delta\log V$, $\Delta\log R$, and $\Delta\log L$ for the four samples based on *I*-band imaging (*top*) and SCII sample based on 2MASS *K*-band imaging (*bottom*). The correlation slopes and their associated errors are reported in Table 4 and are shown at the bottom of each panel in Figure 12. The linear correlation coefficients, *r*, are also shown at the top left corner of each panel. The residual correlations reported in Table 4 supersede those presented in CR99, which differ slightly due to revised corrections to the raw observables.

There is close agreement in the correlated residual solutions of all optical samples, with the general solution

$$\Delta\log V|L/\Delta\log R|L = -0.07 \pm 0.01,$$
$$\Delta\log R|V/\Delta\log L|V = 0.71 \pm 0.02,$$
$$\Delta\log V|R/\Delta\log L|R = 0.31 \pm 0.01.$$

While we do not correct for possible sample incompleteness, the fact that all of our samples, with their very different selection functions, yield similar solutions suggests that any potential selection bias ought to be minimal or cancel out (see discussion in D07). The slopes for the $\Delta\log V|L - \Delta\log R|L$ residuals for all samples are negative (anticorrelated) and low. This residual correlation is statistically different from $\Delta\log V/\Delta\log R = 0$, although only weakly. Note also that galaxies of all morphological types (and barredness, not shown here), scatter normally about the zero line (see Appendix A). FAR00 have also computed the *VL*/*RL* residuals for the UMa sample (Fig. 17, below) and found no correlation for both for LSB and high surface brightness (HSB) galaxies, as do we for that sample (see Table 4 and the bottom left panel of Fig. 18, below).

The weak surface brightness dependence of the *VL* relations has been used to infer the ratio of baryonic to dark mass in the inner parts of galaxies (CR99). D07, however, suggest that changes in the stellar mass-to-light ratio, variations of baryonic-to-stellar mass ratio, bulge formation prescriptions and assumptions about the response of the dark matter halo to the cooling baryons may all contribute to a weaker surface brightness dependence of the *VL* relation.

With $r \simeq 0.5$, the *RV* and *LV* residuals (middle column of Fig. 12) are also weakly correlated. The *VR* and *LR* residual distributions (right column of Fig. 12) are tightly correlated with $r \simeq 0.9$ (a little less at *K*) and relatively small slope errors. This, as we explain below, is simply the *VL* relation recast in differential form.

The correlations between residuals of the *VRL* relations give clues to the contribution of scatter in *V*, *L*, and *R*. Consider a case where scatter exists only in *V*; then the $\Delta\log R|V - \Delta\log L|V$ residuals will be correlated with a slope equal to the log slope of the *RL* relation (i.e., $\sim$0.3). Similarly, for scatter only in *L*, the slope of the $\Delta\log V|L - \Delta\log R|L$ residuals should equal the log slope of the *VR* relation (i.e., $\sim$1); for scatter only in *R*, the slope of the $\Delta\log V|R - \Delta\log L|R$ residuals should equal the log slope of the *VL* relation (i.e., $\sim$0.3).

TABLE 3
ORTHOGONAL FITS FOR THE SCII *K*-BAND SAMPLE

		log *V* vs. log L_K			log $R_{e,K}$ vs. log L_K		
TYPE	*N*	Slope	Zero Point	$\sigma_{\ln V\|L}$	Slope	Zero Point	$\sigma_{\ln R\|L}$
All	360	0.269 ± 0.007	−0.692 ± 0.081	0.126	0.346 ± 0.018	−3.13 ± 0.19	0.291
Sa	56	0.274 ± 0.021	−0.721 ± 0.240	0.129	0.568 ± 0.042	−5.70 ± 0.47	0.266
Sb	131	0.264 ± 0.017	−0.641 ± 0.185	0.130	0.428 ± 0.035	−4.06 ± 0.39	0.265
Sc	166	0.255 ± 0.012	−0.549 ± 0.124	0.118	0.388 ± 0.025	−3.54 ± 0.27	0.261
Sd	7	0.249 ± 0.039	−0.504 ± 0.404	0.081	0.314 ± 0.168	−2.68 ± 1.80	0.358

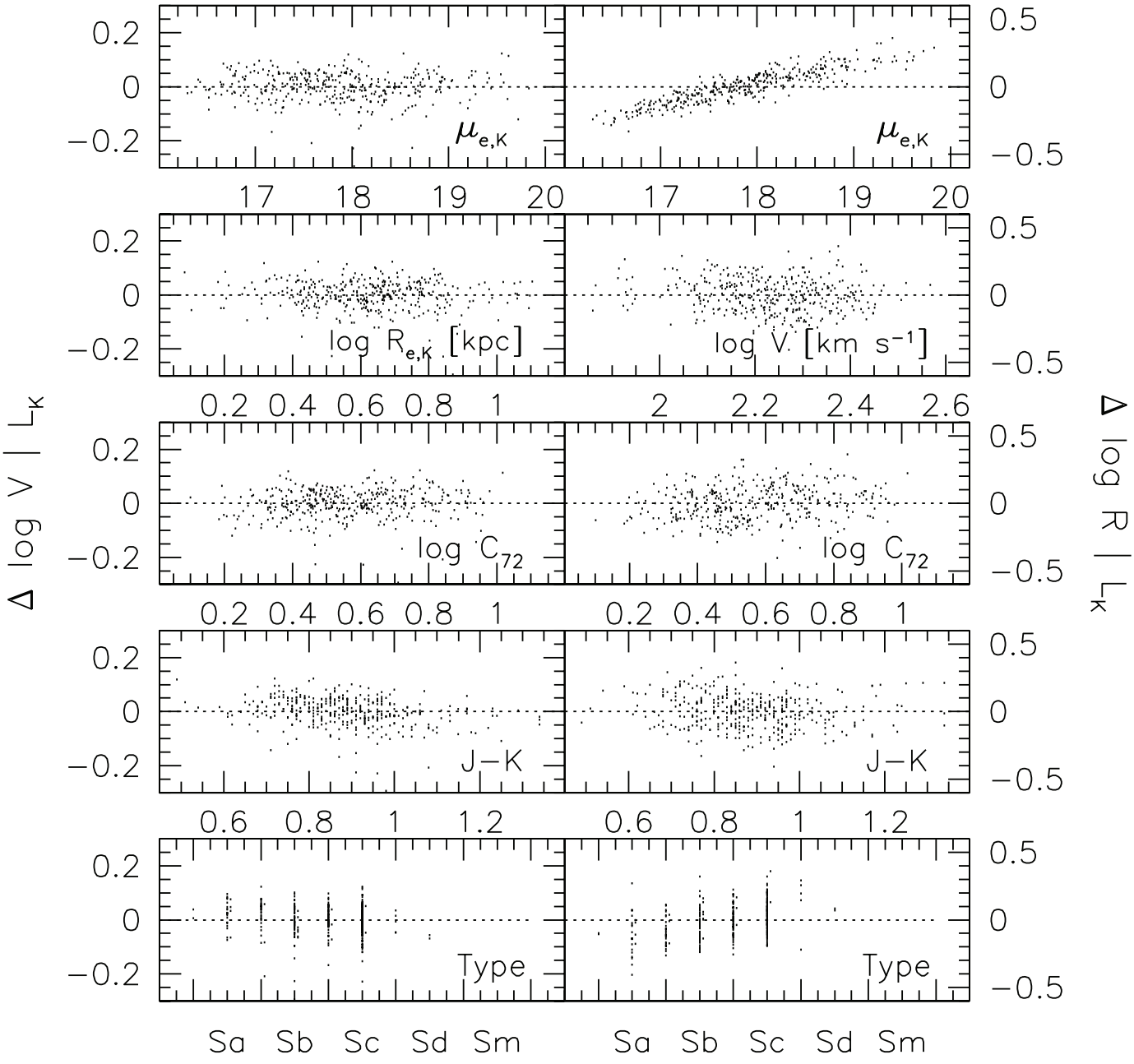

FIG. 11.—Residuals from the 2MASS *VL* (*left*) and *RL* (*right*) relations as a function of effective surface brightness $\mu_{\rm eff}$, effective size ($R_{\rm eff}$), rotation velocity, concentration index, infrared $J - K$ color, and optical morphological type. The sample is grossly incomplete for types later than Sc.

Since there is intrinsic scatter in each of the *VL*, *RL*, and *RV* relations, there must be scatter in at least two of *V*, *L*, and *R*. The case of uncorrelated scatter in *R* and *L*, and no scatter in *V*, would result in a positive $\Delta \log V|L - \Delta \log R|L$ residual correlation, uncorrelated $\Delta \log R|V - \Delta \log L|V$ residuals, and a weak positive $\Delta \log V|R - \Delta \log L|R$ residual correlation. This situation is in clear conflict with all three observed residual correlations. The case with uncorrelated scatter in *V* and *R*, and no scatter in *L* would result in uncorrelated $\Delta \log V|L - \Delta \log R|L$ residuals, $\Delta \log V|R - \Delta \log L|R$ residuals with slope $\sim$0.3, and positively correlated $\Delta \log R|V - \Delta \log L|V$ residuals. This latter is indeed in excellent agreement with the observations. Thus, in the simplest interpretation of the residual correlations, the scatter in the *VL* and *RL* relations is fully independent. However, as discussed in D07, reproducing independent *VL* and *RL* relations is nontrivial as the various theoretically expected sources of scatter in $V|L$ and $R|L$ often result in correlated *V* and *R* scatter.

We conclude this section with a discussion of the color dependence of residual correlations. As discussed in § 2.3, the *VRL* relations show a dependence on color and morphological type. Since both color and morphological type depend on luminosity and velocity, a most robust way to look for a color dependence of the *VRL* relations is to compare the *VRL* residuals with residuals of the color-luminosity and color-velocity relations. This is shown in Figure 13. The upper panels show the $V - I$ color-luminosity and $V - I$ color-rotation velocity relations. The middle panels show the *VL* residuals versus color residuals. The dashed lines show the predicted correlation slope for scatter in color at

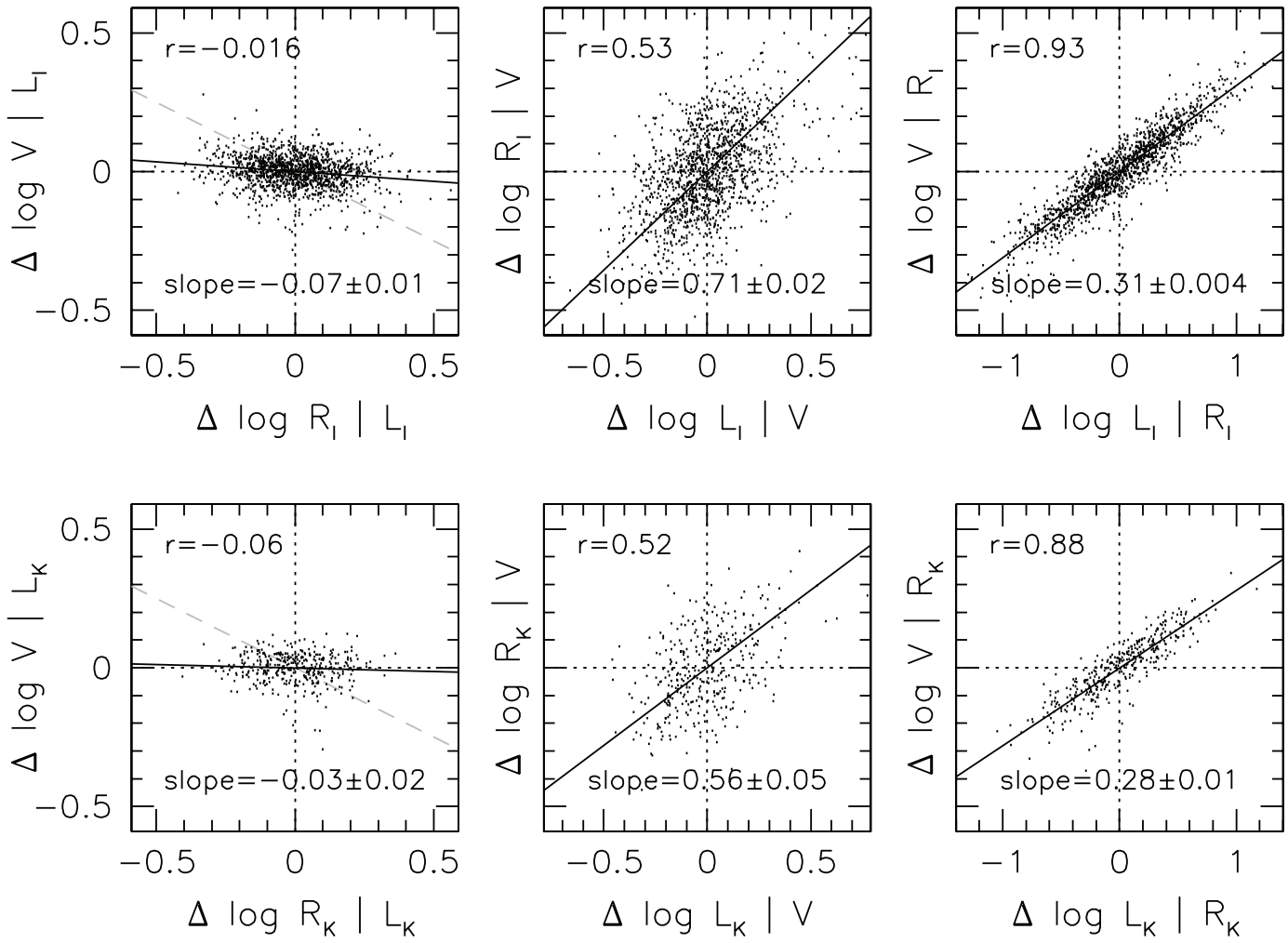

FIG. 12.—Correlations between the residuals of the *VRL* relations for the *I*-band sample (*top*) and *K*-band sample (*bottom*). The best-fitting slopes with 1 σ uncertainty and correlation coefficients are given in the lower and upper left corner of each panel. There is only a weak correlation between $V|L$ and $R|L$ (*left*) compared to the prediction for pure disk only model (dashed line with slope −0.5). There is a significant correlation between the $L|V$ and $R|V$ residuals (*middle*), and even tighter correlation between $V|R$ and $L|R$, which is simply the *VL* relation in differential form.

a given stellar mass, assuming $\log M_*/L_I \propto 1.26(V-I)$ from stellar population models (Portinari et al. 2004), and that scatter in color is uncorrelated with V and R. For the $\Delta\log V|L_I - \Delta(V-I)|L_I$ residuals, the observed correlation is weak but of the same sign as expected (from the stellar population models), in agreement with P07. This further confirms that scatter in color is a contributing, but not dominant, source of scatter in the *VL* relation. However, the $\Delta\log L_I|V - \Delta(V-I)|V$ residuals are perfectly uncorrelated, also in agreement with P07. This is explained if scatter in the velocity-stellar mass relation depends on color, in the sense that redder galaxies of a given stellar mass rotate slower. However, this strikes against theoretical expectations that redder galaxies of a given total luminosity should rotate faster.

We also find that the $\Delta\log R|L_I - \Delta(V-I)|L_I$ residuals have only a weak correlation, but of opposite sign to that expected. This suggests that the scatter in the size-stellar mass relation depends on color, with redder galaxies of a given stellar mass being smaller. This is expected from theoretical galaxy formation models (Bell et al. 2003a). Finally, the $\Delta\log R|V - \Delta(V-I)|V$ residuals

TABLE 4
VLR RESIDUAL CORRELATIONS

		$\Delta\log V\|L$ vs. $\Delta\log R\|L$		$\Delta\log R\|V$ vs. $\Delta\log L\|V$		$\Delta\log V\|R$ vs. $\Delta\log L\|R$	
SAMPLE	N	Slope	r	Slope	r	Slope	r
All	1303	−0.07 ± 0.01	(−0.16)	0.71 ± 0.02	(+0.53)	0.31 ± 0.01	(+0.93)
MAT	545	−0.11 ± 0.03	(−0.17)	0.57 ± 0.04	(+0.59)	0.32 ± 0.01	(+0.90)
SCII	468	−0.09 ± 0.02	(−0.20)	0.84 ± 0.08	(+0.53)	0.32 ± 0.01	(+0.94)
Shellflow	252	−0.08 ± 0.03	(−0.18)	0.78 ± 0.09	(+0.52)	0.32 ± 0.01	(+0.93)
UMa	38	−0.06 ± 0.08	(−0.14)	0.77 ± 0.17	(+0.48)	0.31 ± 0.02	(+0.93)
SCII K	360	−0.03 ± 0.02	(−0.06)	0.56 ± 0.05	(+0.52)	0.28 ± 0.01	(+0.88)

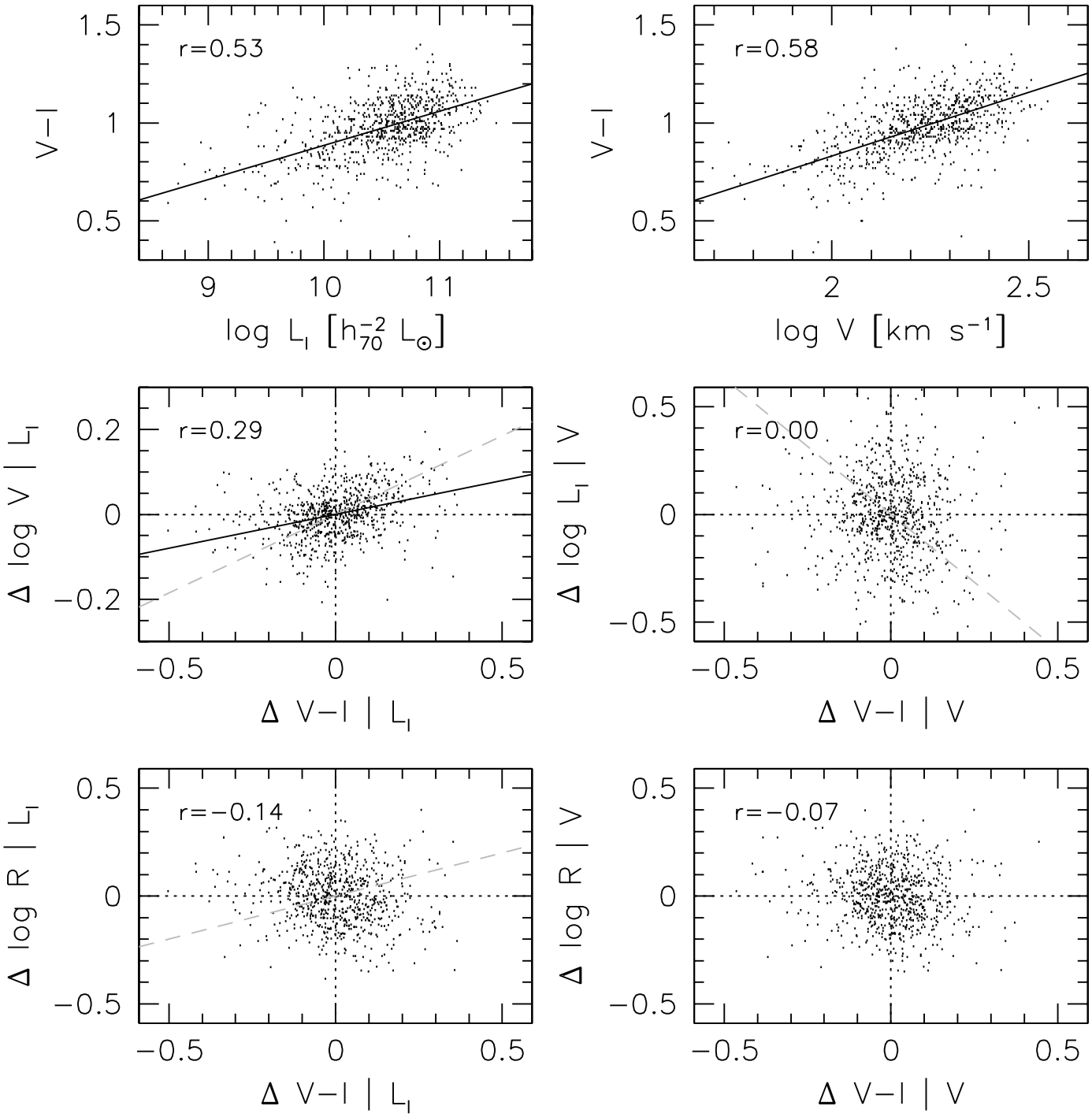

FIG. 13.—Correlation residuals of the *I*-band relations with $V - I$ color. The top panels show the color-luminosity (*left*) and color-rotation velocity (*right*) relations. The middle panels show the residuals of the *VL* relation vs. the color residuals at constant *L* (*left*) and constant *V* (*right*). The bottom panels show the size residuals vs. the color residuals at constant *L* (*left*) and constant *V* (*right*). The dashed lines give predictions based on scatter in color at fixed stellar mass and assuming, based on stellar population models, that color is related to stellar mass-to-light ratio.

show no correlation, but luminosity also does not play any role in this correlation, and therefore no dependence on colors is expected here.

4. DISCUSSION

The collection of some of the most extensive existing databases of galaxy structural and dynamical parameters at *I* and *K* bands has enabled us to determine the following major observational results:

i. The *I*-band scaling relations of spiral galaxies, obtained by linear regressions of *V* on *L* and *R* on *L*, are

$$V \propto L_I^{0.29\pm0.01}, \qquad R_d \propto L_I^{0.32\pm0.01}, \qquad R_d \propto V^{1.10}.$$

ii. The 2MASS *K*-band scaling relations of bright SCII galaxies differ slightly (due to selection effects) with

$$V \propto L_K^{0.27\pm0.01}, \qquad R_{e,K} \propto L_K^{0.35\pm0.02}, \qquad R_{e,K} \propto V^{1.29}.$$

The slightly shallower log slopes of the *VL* relations from the *I* to *K* band are expected based on the observed trend of color with luminosity. However, the *K*-band *RL* and *RV* relations are biased to higher slopes due to the surface brightness bias of the 2MASS catalog for extended objects. A study of scaling relations based on deeper IR survey data (e.g., UKIDSS; Hewett et al. 2006) should recover shallower slopes, comparable to those measured here for *I*-band data, for the infrared *RL* and *RV* relations.

iii. The log slopes of the *I*- and *K*-band *VL* and *RL* relations show a dependence on morphological type, with steeper slopes for earlier type disk galaxies, especially so for the *RL* relation.

iv. The *I*-band *VL* relation shows a dependence on color in the direction expected from simple stellar population synthesis models. However, the *RL* relation shows a trend (albeit weak) in the opposite direction, which is most simply interpreted as smaller galaxies at a given stellar mass being slightly redder.

v. The *VL* relation shows no dependence on size or surface brightness at both *I* and *K* bands.

vi. The $\Delta \log V|L - \Delta \log R|L$ residuals are weakly anticorrelated with correlation coefficient $r \simeq -0.2$ and slope -0.07 ± 0.01. Unlike CR99, we showed in Dutton et al. (2007) that this result does not uniquely imply that most spiral disks have submaximal fraction of luminous to dark matter.

vii. The $\Delta \log R|V - \Delta \log L|V$ residuals are weakly correlated with correlation coefficient $r \simeq 0.5$ and slope $\simeq 0.7$. Together with the weak $\Delta \log V|L - \Delta \log R|L$ residual correlation, this suggests that scatter in velocity and size dominate the scatter in the *VL* and *RL* relations, respectively.

viii. The $\Delta \log V|R - \Delta \log L|R$ residuals are strongly correlated with correlation coefficient $r \simeq 0.9$ and slope $\simeq 0.3$. This is the *VL* relation recast in differential form.

The slopes zero points and scatter of the *VL*, *RL*, and *RV* relations can be broadly understood in the context of disk galaxies embedded in dark matter halos as discussed in Appendix B and in more detail in Dutton et al. (2007). However, accurately reproducing the zero point and surface brightness independence of the *VL* relation, as well as the galaxy number density, may require a departure from the standard assumptions governing the formation of disk galaxies.

In order to make further progress in constraining disk galaxy formation models from the *VRL* relations, a large ($N \gtrsim 1000$) sample of galaxies with deep multiwavelength imaging (near-IR is essential), high spatial and spectral resolution 1D and 2D spectroscopy (with CO, Hα, and H I maps), controlled selection criteria, accurate and homogeneous measurements of structural parameters, and stellar and baryonic masses, is needed. Ideally, chemical information should be available to constrain stellar population effects.

We acknowledge useful conversations and suggestions from Eric Bell, Roelof de Jong, Hans-Walter Rix, Marc Verheijen, and Ben Weiner. Michael McDonald and Dan Zucker kindly helped with the extraction of Petrosian magnitudes from the SDSS database. S. C. wishes to acknowledge his colleagues on the Shellflow team (Marc Postman, David Schlegel, and Michael Strauss) for permission to use and release unpublished data. S. C. and L. A. M. acknowledge financial support from the National Science and Engineering Council of Canada. A. A. D. acknowledges support from the Swiss National Science Foundation (SNF) and from the National Science Foundation Grant AST-0507483. A. D. acknowledges support by the US-Israel Bi-National Science Foundation grant 98-00217, the German-Israel Science Foundation grant I-629-62.14/1999, and NASA ATP grant NAG5-8218. D. H. M. acknowledges support from the National Aeronautics and Space Administration (NASA) under LTSA Grant NAG5-13102 issued through the Office of Space Science. S. C. would also like to thank the Max-Planck-Institut für Astronomie in Heidelberg and the Max-Planck-Institut für Astrophysik in Munich for their hospitality while part of this paper was conceived.

This research has made use of (1) the NASA/IPAC Extragalactic Database (NED) which is operated by the Jet Propulsion Laboratory, California Institute of Technology, under contract with the National Aeronautics and Space Administration, as well as NASA's Astrophysics Data System; (2), the Two Micron All Sky Survey, which is a joint project of the University of Massachusetts and the Infrared Processing and Analysis Center/California Institute of Technology, funded by the National Aeronautics and Space Administration and the National Science Foundation; and (3) the Sloan Digital Sky Survey (SDSS). Funding for the creation and distribution of the SDSS Archive has been provided by the Alfred P. Sloan Foundation, the Participating Institutions, the National Aeronautics and Space Administration, the National Science Foundation, the US Department of Energy, the Japanese Monbukagakusho, and the Max Planck Society. The SDSS Web site is http://www.sdss.org/. The SDSS is managed by the Astrophysical Research Consortium (ARC) for the Participating Institutions. The Participating Institutions are the University of Chicago, Fermilab, the Institute for Advanced Study, the Japan Participation Group, The Johns Hopkins University, Los Alamos National Laboratory, the Max-Planck-Institut für Astronomie (MPIA), the Max-Planck-Institut für Astrophysik (MPA), New Mexico State University, University of Pittsburgh, Princeton University, the United States Naval Observatory, and the University of Washington.

APPENDIX A

I-BAND SCALING RELATIONS AND RESIDUAL CORRELATIONS FOR THE FOUR MAIN SAMPLES

This Appendix presents the separate distributions for the *VRL* scaling relations of the SCII, MAT, Shellflow, and UMa samples. These are shown, respectively, in Figures 14, 15, 16, and 17. The axis limits are the same in all figures and the fits shown are those for the full combined sample (see Fig. 3).

Figure 18 shows the residual correlations for combinations of $\Delta \log V$, $\Delta \log R$, and $\Delta \log L$ for the four samples based on *I*-band imaging. The colored point types have the same morphological dependence as in Figure 3. All four samples give consistent residual correlations, namely a very weak $\Delta \log V|L - \Delta \log R|L$ correlation (analogous to the surface brightness and size independence of the *VL* relation), a weak positive $\Delta \log R|V - \Delta \log L|V$ correlation, and a strong positive $\Delta \log V|R - \Delta \log L|R$ correlation (the differential *VL* relation).

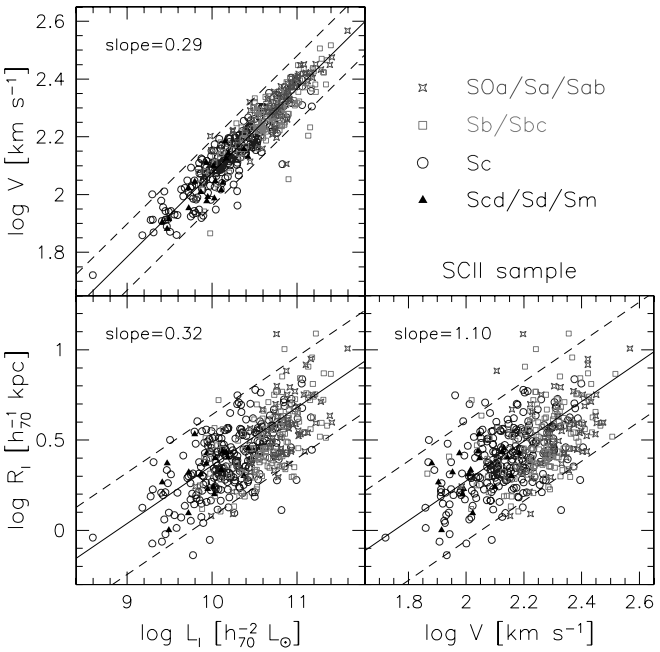

FIG. 14.—Scaling relations for SCII galaxies. Line widths are measured from Hα rotation curves and disk scale lengths are measured using the marking the disk technique (see text). Luminosities are computed from fully corrected *I*-band magnitudes. Unlike Dale et al. (1999), the luminosities do not include any correction for morphological type dependence. The solid black lines and reported slopes correspond the orthogonal fits to the combined data set. The point types and colors correspond to the Hubble classification from the authors (Dale et al. 1999). [*See the electronic edition of the Journal for a color version of this figure*.]

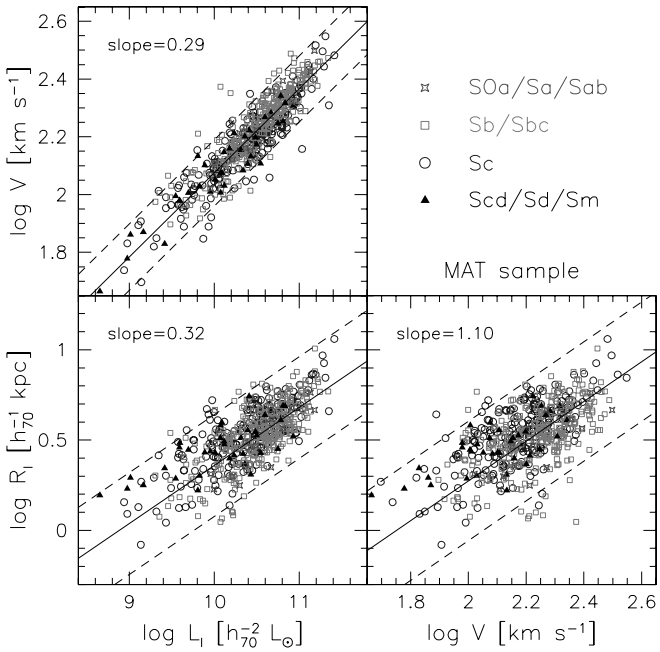

FIG. 15.—Scaling relations for MAT galaxies. Line widths are measured from Hα rotation curves and disk scale lengths are measured from bulge-to-disk decompositions. Luminosities are computed from fully corrected *I*-band magnitudes. The fits are as in Fig. 14. Hubble types are taken from the NASA Extragalactic Data Base. [*See the electronic edition of the Journal for a color version of this figure*.]

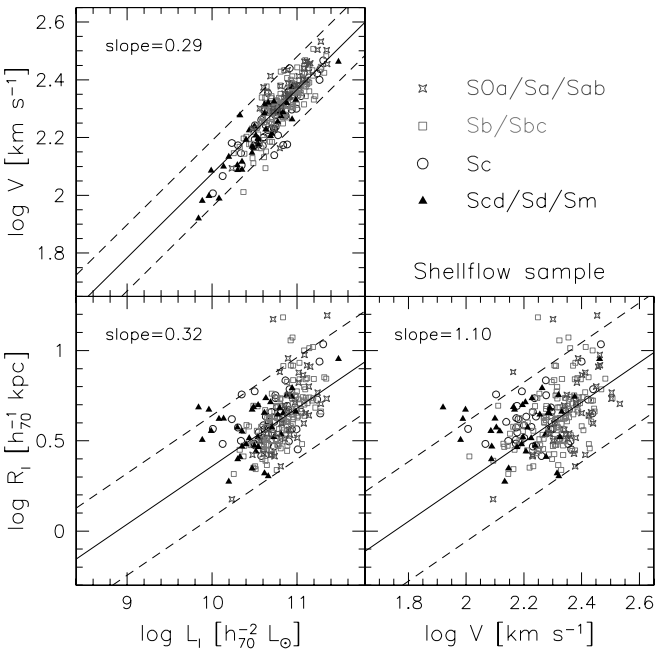

FIG. 16.—Scaling relations for Shellflow galaxies. Line widths are measured from Hα rotation curves and disk scale lengths are measured from bulge-to-disk decompositions. Luminosities are computed from fully corrected *I*-band magnitudes. Fits and point types are as in Fig. 14. [*See the electronic edition of the Journal for a color version of this figure*.]

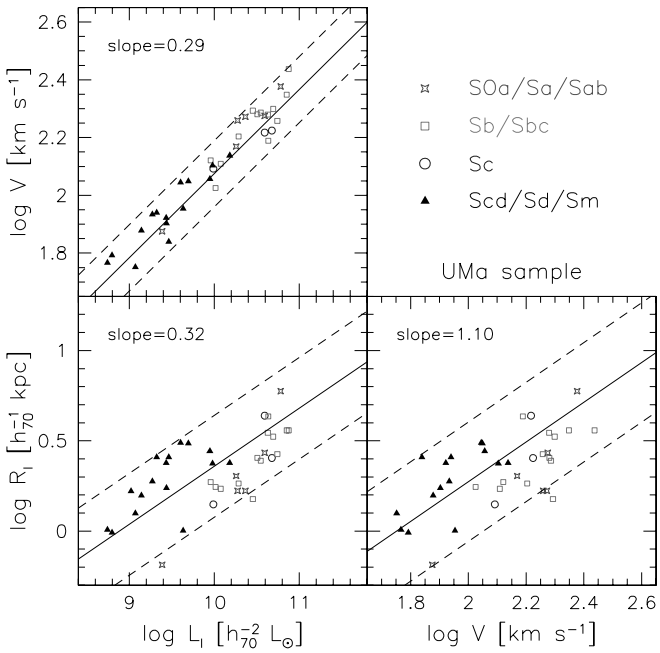

FIG. 17.—Scaling relations for UMa galaxies. Line widths are measured from H I synthesis rotation curves and disk scale lengths are measured using the marking the disk technique (see text). Luminosities are computed from fully corrected *I*-band magnitudes. Fits and point types are as in Fig. 14. [*See the electronic edition of the Journal for a color version of this figure*.]

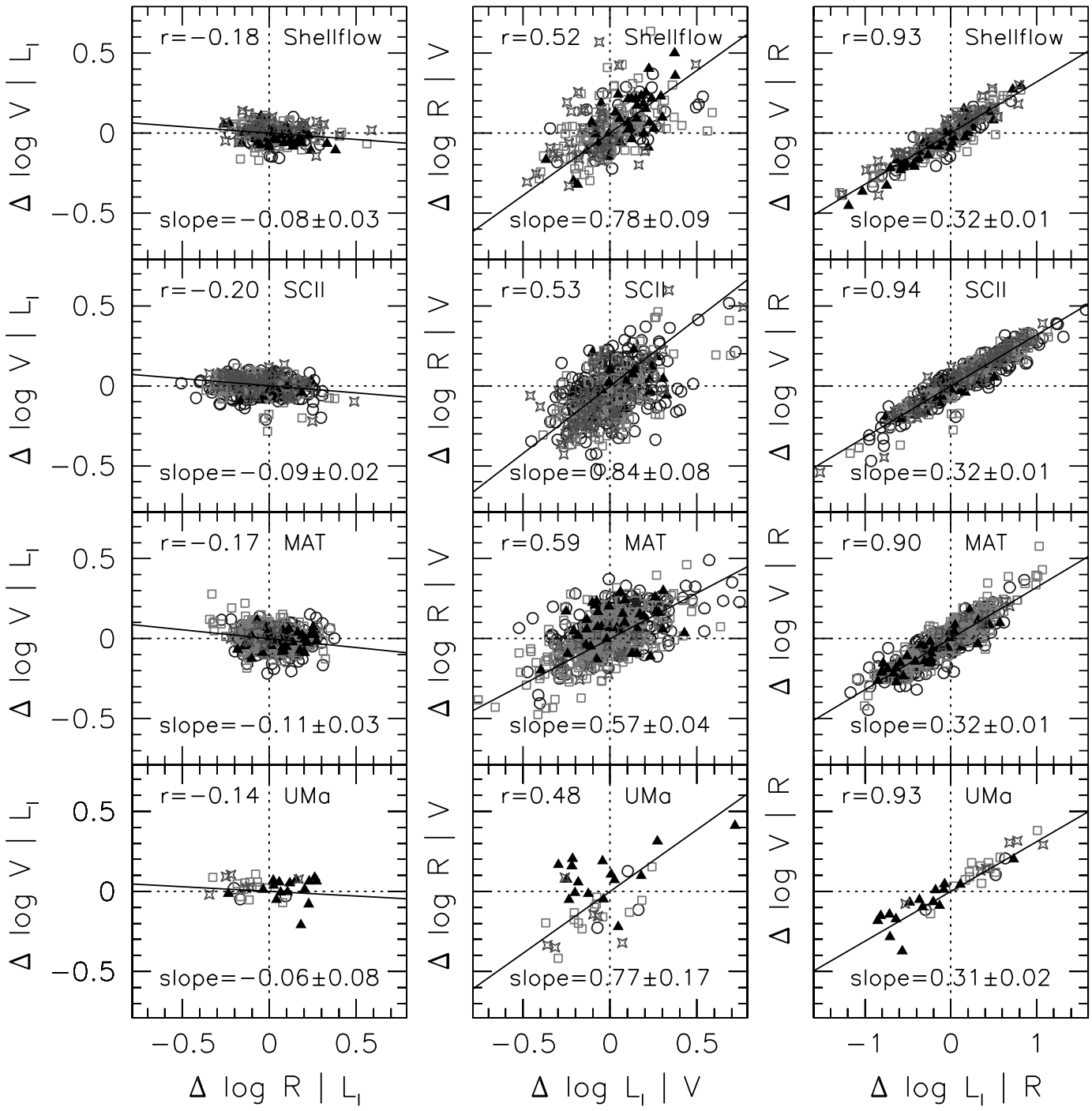

FIG. 18.—Correlation residuals from the mean relation at fixed virial quantity for the Shellflow, SCII, MAT, and UMa samples. Symbols are as in Fig. 3. Galaxies of all shapes and types (barred and unbarred, early and later types) obey the same surface brightness independent scaling relations. The residual distribution for $\Delta \log V/\Delta \log R$ of all three samples is flat for barred and unbarred galaxies of all Hubble types and luminosities. The middle figures show a weak correlation between L and R, and the figures on the right side recast the VL relation in its differential form. [*See the electronic edition of the Journal for a color version of this figure.*]

APPENDIX B

ON THE ORIGIN OF DISK GALAXY SCALING RELATIONS

The mean observed trends between $V_{\rm obs}$, L, and R_d at I band are given by the following VL, RL, and RV relations:

$$V_{\rm obs} \propto L^{0.29}, \qquad R_d \propto L^{0.32}, \qquad R_d \propto V_{\rm obs}^{1.10}. \tag{B1}$$

In the spirit of the spherical-collapse model (Gunn & Gott 1972), one can define the virial radius, $R_{\rm vir}$, of a collapsed, virialized gravitational body as the radius inside of which the average density is a factor $\Delta_{\rm vir}$ times the critical density of the universe (the value

of $\Delta_{\rm vir}$ depends on redshift and cosmology; see e.g., Eke et al. 1998; Bryan & Norman 1998). Thus, one can write the virial mass, $M_{\rm vir}$, as

$$M_{\rm vir} = \frac{4}{3}\pi R_{\rm vir}^3 \Delta_{\rm vir} \rho_{\rm crit}, \tag{B2}$$

where $\rho_{\rm crit}$ is the critical density of the universe at a given z, and is given by

$$\rho_{\rm crit} = \frac{3H(z)^2}{8\pi G}, \tag{B3}$$

where $H(z)$ is the Hubble constant at redshift z. From the virial theorem, the circular velocity at the virial radius, $V_{\rm vir}$, is given by

$$V_{\rm vir}^2 = \frac{GM_{\rm vir}}{R_{\rm vir}}. \tag{B4}$$

Combining equations (B2)–(B4) and setting $H(z) = 100\ h$ km s^{-1} Mpc^{-1}, we obtain

$$M_{\rm vir} = R_{\rm vir}^3\ h^2\ \left(\frac{\Delta_{\rm vir}}{200}\right)\frac{1}{G}, \tag{B5}$$

$$V_{\rm vir} = R_{\rm vir}\ h\ \left(\frac{\Delta_{\rm vir}}{200}\right)^{1/2}, \tag{B6}$$

$$M_{\rm vir} = V_{\rm vir}^3\ h^{-1}\ \left(\frac{\Delta_{\rm vir}}{200}\right)^{-1/2} G, \tag{B7}$$

where G has units of (km s^{-1})^2 kpc $M_\odot^{-1}$, $M_{\rm vir}$ has units of $M_\odot$, $R_{\rm vir}$ has units of kpc, and $V_{\rm vir}$ has units of km s^{-1}.

Thus, if $M_{\rm vir}/L$, $R_{\rm vir}/R_d$, and $V_{\rm vir}/V_{\rm obs}$ are roughly constant for different galaxy types (i.e., not significantly correlated with either of the virial quantities), these virial relations are all that is required to explain the observed scaling relations of disk galaxies. However, there are many reasons to expect significant variation in $M_{\rm vir}/L$, $R_{\rm vir}/R_d$, and $V_{\rm vir}/V_{\rm obs}$. Below we realize these variations in terms of galaxy formation theory.

The virial mass-to-light ratio can be written as

$$M_{\rm vir}/L = \frac{\Upsilon_*}{f_{\rm bar}\epsilon_{\rm gf}\epsilon_{\rm sf}} = \frac{\Upsilon_d}{m_d}, \tag{B8}$$

where $\Upsilon_* \equiv M_*/L$ is defined as the stellar mass-to-light ratio, $f_{\rm bar}$ is the baryonic mass fraction of the universe ($f_{\rm bar} = \Omega_{\rm b}/\Omega_M \simeq 0.15$ for a ΛCDM cosmology), $\epsilon_{\rm gf}$ is the galaxy formation efficiency that describes what fraction of the baryonic mass inside the halo ultimately ends up in the disk, and $\epsilon_{\rm sf}$ is the star formation efficiency that describes what fraction of the disk mass ends up in the form of stars. We combine $f_{\rm bar}$ and $\epsilon_{\rm gf}$ into the disk mass fraction, m_d, and Υ_* and $\epsilon_{\rm sf}$ into the disk mass to light ratio, Υ_d.

The virial relation $V_{\rm vir} \propto M_{\rm vir}^{1/3}$ is thus related to the observed VL relation by the quantity

$$\mathcal{C}_{VL} \equiv \frac{V_{\rm obs}}{V_{\rm vir}}\left(\frac{\Upsilon_d}{m_d}\right)^{1/3}. \tag{B9}$$

In order to reproduce the observed VL relation $V_{\rm obs} \propto L^{\alpha_{VL}}$, $\mathcal{C}_{VL}$ must be proportional to $L^{\alpha_{VL}-1/3}$, and has to reveal an amount of scatter that matches that of the observed VL relation.

In the standard model for disk formation, set forth by Fall & Efstathiou (1980), Dalcanton et al. (1997), and MMW98, the relation between R_d and $R_{\rm vir}$ derives from the acquisition and conservation of (specific) angular momentum by the baryons, when cooling to form a centrifugally supported disk. The total angular momentum of a virialized system is conveniently expressed by the dimensionless spin parameter (Bullock et al. 2001a):

$$\lambda \equiv \frac{J_{\rm vir}}{\sqrt{2}M_{\rm vir}R_{\rm vir}V_{\rm vir}}. \tag{B10}$$

For an exponential disk embedded in a dark matter halo, the total angular momentum is given by

$$J_d = 2\pi\int_0^{R_{\rm vir}} \Sigma(R)V_c(R)R^2\,dR = M_d R_d V_{\rm vir} f_V, \tag{B11}$$

where $\Sigma(R)$ and $V_c(R)$ are the surface density and circular velocity of the disk, and (MMW98)

$$f_V = \int_0^\infty e^{-u} u^2 \frac{V_c(R_d u)}{V_{\rm vir}}\, du \tag{B12}$$

is a dimensionless number [e.g., $f_V = 2$ if $V_c(R) = V_{\rm vir}$]. The specific angular momentum of the disk is related to that of the halo via

$$\lambda_d = \lambda \left(\frac{J_d}{J_{\rm vir}}\right)\left(\frac{M_{\rm vir}}{M_d}\right) = \lambda \left(\frac{j_d}{m_d}\right). \tag{B13}$$

If disk formation occurred under conservation of specific angular momentum, as generally assumed, then $\lambda_d = \lambda$. Independent of this particular assumption one therefore finds that (MMW98)

$$\frac{R_d}{R_{\rm vir}} = \sqrt{2}\frac{\lambda_d}{f_V}. \tag{B14}$$

Thus, the virial relation $R_{\rm vir} \propto V_{\rm vir}$ is related to the observed RV relation by the quantity

$$\mathcal{C}_{RV} \equiv \frac{\lambda_d}{f_V}\left(\frac{V_{\rm vir}}{V_{\rm obs}}\right). \tag{B15}$$

In order to reproduce the observed RV relation $R_d \propto V^{\alpha_{RV}}$, $\mathcal{C}_{RV}$ must be proportional to $V_{\rm obs}^{\alpha_{RV}-1}$, and has to reveal an amount of scatter that matches that of the observed RV relation.

Similarly, the virial relation $R_{\rm vir} \propto M_{\rm vir}^{1/3}$ is related to the observed RL relation by the quantity

$$\mathcal{C}_{RL} \equiv \frac{\lambda_d}{f_V}\left(\frac{\Upsilon_d}{m_d}\right)^{1/3}. \tag{B16}$$

In order to reproduce the observed RL relation $R_d \propto L^{\alpha_{RL}}$, $\mathcal{C}_{RL}$ must be proportional to $L^{\alpha_{RL}-1/3}$, and has to reveal an amount of scatter that matches that in the RL relation observed.

Thus, the challenge for galaxy formation theories is to understand how to meet the constraints on $\mathcal{C}_{VL}$, $\mathcal{C}_{RV}$, and $\mathcal{C}_{RL}$ derived here. That this is not a trivial matter becomes clear if one takes into consideration that (1) both m_d and Υ_d depend extremely sensitively on the efficiencies of cooling, star formation, and feedback, and are thus expected to be strongly correlated with $M_{\rm vir}$ and λ (e.g., van den Bosch 2002), and (2) both $V_{\rm obs}/V_{\rm vir}$ and f_V depend, in a convoluted way, on λ, m_d, adiabatic contraction, and initial halo concentration (e.g., D07), which itself depends on halo mass (e.g., Bullock et al. 2001b).

In summary, while the virial relations of dark matter halos provide a natural framework for understanding the observed scaling relations of disk galaxies, a direct linkage between the slopes of the observed and virial relations ignores the many physical processes that take place during galaxy formation.

APPENDIX C

AN ALTERNATIVE DERIVATION OF THE TULLY-FISHER RELATION

Two simple predictions for the Tully-Fisher (VL or TF) relation have been used in the past, one with a log slope of 3 (-7.5 in magnitudes), and the other with a log slope of 4 (-10 in magnitudes). Here we compare both predictions and show that they are related to one another.

From Appendix B, we have

$$L = V_{\rm obs}^3\, h^{-1} \left(\frac{\Delta_{\rm vir}}{200}\right)^{-1/2} \frac{m_d}{\Upsilon_d}\left(\frac{V_{\rm vir}}{V_{\rm obs}}\right)^3 G \propto V_{\rm obs}^3 \mathcal{C}_{VL}. \tag{C1}$$

This is a TF relation with log slope of 3, if $\mathcal{C}_{VL}$ is independent of $V_{\rm obs}$ (see also Dalcanton et al. 1997; MMW98; van den Bosch 1998; Syer et al. 1999).

In contrast, several authors in the past have predicted that the TF relation should have a log slope of 4 (e.g., Sargent et al. 1977; Aaronson et al. 1979; Salucci et al. 1993; Sprayberry et al. 1995; Zwaan et al. 1995). Their argument goes as follows. Assume that the disk surface brightness is described by an exponential function of the form

$$I(r) = I_0 \exp(-r/R_d), \tag{C2}$$

where R_d is the disk scale length and I_0 is the disk central surface brightness. The total luminosity of the disk is

$$L = 2\pi I_0 R_d^2. \tag{C3}$$

Assuming that one measures the rotation velocity $V_{\rm obs}$ at a radius $r = sR_d$, and that the gas and stars in the disk move on circular orbits,

$$V_{\rm obs}^2 = \frac{GM(r)}{r}, \tag{C4}$$

where $M(r)$ is the total mass within radius r. We can define the total mass-to-light ratio[6]

$$\tilde{\Upsilon}(r) \equiv \frac{M(r)}{L} = \frac{M_d(r) + M_h(r)}{L}, \tag{C5}$$

square equation (C4), and then use equations (C3) and (C5) to obtain

$$L = V_{\rm obs}^4 \frac{s^2}{I_0 \tilde{\Upsilon}^2(r)} \frac{1}{2\pi G^2}. \tag{C6}$$

This is a TF relation with a log slope of 4, as long as $I_0\tilde{\Upsilon}^2(r)$ is independent of $V_{\rm obs}$ and one measures the rotation velocity at a constant number of scale lengths.[7] The scatter is determined purely by the variation in $I_0\tilde{\Upsilon}^2(r)$. This was emphasized by Zwaan et al. (1995), who, from the finding that both HSB and LSB spirals follow the same TF relation, concluded that LSB galaxies must have much larger values of $\tilde{\Upsilon}^2(r)$ than their HSB counterparts.

The TF relations in equations (C1) and (C6) thus predict a different log slope. The cause of this apparent paradox lies in the fact that I_0 and $V_{\rm obs}$ are *not* independent. From equations (B5), (B14), and (C3), we derive the relation between surface brightness and observed rotation velocity

$$I_0 = V_{\rm obs}\ h\ \frac{m_d}{\Upsilon_d} \left(\frac{f_V}{\lambda_d}\right)^2 \left(\frac{V_{\rm vir}}{V_{\rm obs}}\right) \frac{G}{4\pi}. \tag{C7}$$

Substituting this into equation (C6) yields a TF relation with a slope of 3, as long as

$$\mathcal{C}_{VL} = \frac{s^2}{\tilde{\Upsilon}^2(r)} \frac{\Upsilon_d}{m_d} \frac{\lambda_d^2}{f_V^2} \frac{V_{\rm obs}}{V_{\rm vir}} \tag{C8}$$

is independent of $V_{\rm obs}$. Rather than squaring equation (C4), a simpler expression results from substituting the relation between R_d and $V_{\rm obs}$ (see Appendix B) into equation (C4), thus resulting in

$$L = V_{\rm obs}^3\ h^{-1}\ \frac{s}{\tilde{\Upsilon}(r)} \frac{\lambda_d}{f_V} \frac{V_{\rm vir}}{V_{\rm obs}} \left(\frac{\Delta_{\rm vir}}{200}\right)^{-1/2}. \tag{C9}$$

This is a TF relation with a slope of 3, as long as

$$\mathcal{C}_{VL} = \frac{s}{\tilde{\Upsilon}(r)} \frac{\lambda_d}{f_V} \frac{V_{\rm vir}}{V_{\rm obs}} \tag{C10}$$

is independent of $V_{\rm obs}$.

Thus, the two theoretical predictions of the TF relation, with log slopes 3 and 4, are directly related. However, while equations (C1) and (C9) have an underlying TF slope of 3, variation of $\mathcal{C}_{VL}$ with $V_{\rm obs}$ (or L) will result in a steeper or shallower slope. For example, stellar mass-to-light ratios increase with $V_{\rm obs}$ (e.g., D07), and stellar mass fractions increase with $V_{\rm obs}$ (e.g., Kannappan 2004). This results in the steepest slope for the stellar mass TF relation, an intermediate slope for the baryonic mass TF relation, and the shallowest slope for the blue luminosity TF relation (e.g., Bell & de Jong 2001). The slope of the TF relation will also depend on the velocity measurement, since the shape of galaxy rotation curves changes systematically with luminosity (e.g., C97; Catinella et al. 2006).

APPENDIX D

SDSS COLORS FOR GALAXY CLASSIFICATION

The need for dynamical and color information is crucial for any study of galaxy scaling relations. However, of all the available samples with *homogeneous* dynamical measurements (e.g., rotation curves) considered here, digital colors are only available for the Shellflow and UMa samples with *VI* and *BRI* imaging, respectively. The MAT and SCII galaxy magnitudes were imaged only at *I* band. In order to augment the available color base, we computed, in CR99, a $B - I$ color term for MAT galaxies using B band magnitudes for the RC3 (de Vaucouleurs et al. 1991). However, RC3 magnitudes are inherently uncertain with $\Delta m \simeq 0.2$ mag (Courteau 1996).

[6] We use the subscripts "d" and "h" to refer to the disk and dark matter halo, respectively.

[7] Note that this derivation can be generalized to an arbitrary surface brightness profile by replacing the central surface brightness, I_0, with the effective surface brightness, $I_{\rm eff}$, and the disk scale length, R_d, with the effective (i.e., half-light) size, $R_{\rm eff}$.

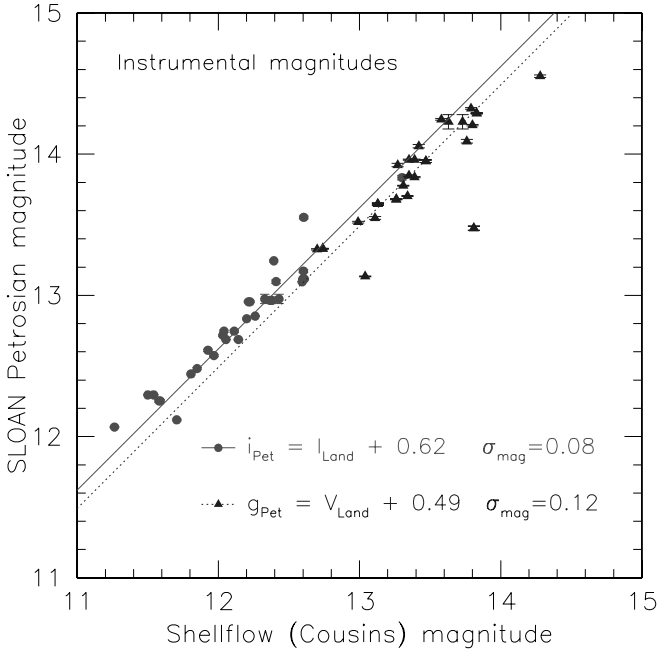

FIG. 19.—Comparison of raw SDSS (Petrosian) and Shellflow (Cousins) magnitudes. The two photometry data sets are derivable from one another, independent of a color term at least over the Shellflow magnitude range. [*See the electronic edition of the Journal for a color version of this figure*.]

We can extract SDSS *g* and *i* magnitudes (as proxy for *V* and *I* magnitudes) for the galaxies that overlap with our northern samples. We do this for Shellflow and SCII galaxies in order to map the SDSS system onto the Landolt/Cousins system on which Shellflow and SCII magnitudes are based. We compare in Figures 19 and 20 instrumental Petrosian magnitudes from the SDSS fifth release against instrumental magnitudes for 31 Shellflow and 39 SCII galaxies. The comparison of instrumental magnitudes avoids any differences due to extinction and *k*-corrections. Besides zero-point offsets, the *g* and *i* Petrosian magnitudes scale linearly with the *V* and *I* Cousins magnitudes in Shellflow. The same is true for SCII at near-infrared bands. Because the transformation slopes at *I* band are the same for Shellflow and SCII, we make the assumption that the transformation slopes at visual bands will also be similar. We also assume a monochromatic zero-point difference between the Shellflow and SCII magnitude systems of 0.13 mag.

We compute transformations for the SDSS Petrosian *g* magnitudes into Cousins magnitudes using $g_{\rm Pet} = V_{\rm Land} + 0.36$ for the SCII galaxies that overlap with the SDSS/DR5 database. The new instrumental "*V*" magnitudes from SDSS for 39 SCII galaxies were corrected the same way as the *I*-band magnitudes but using an extinction dependence $A_V = 3.24$, instead of $A_I = 1.96$, and the Poggianti (1997) formulation for the *V*-band *k*-correction.

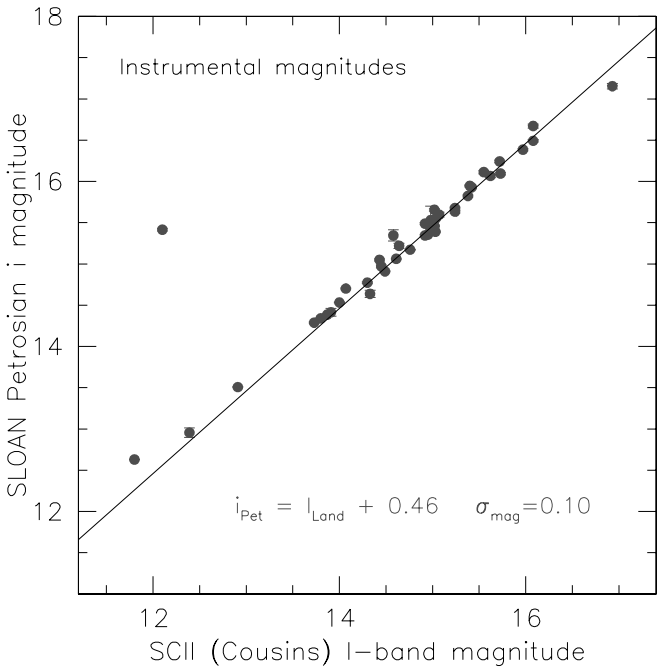

FIG. 20.—Comparison of raw SDSS (Petrosian) and SCII (Cousins) magnitudes. The linear transformation of magnitudes holds over nearly 3 mag, independent of a color term. [*See the electronic edition of the Journal for a color version of this figure*.]

REFERENCES

Aaronson, M., Huchra, J., & Mould, J. 1979, ApJ, 229, 1
Aaronson, M., & Mould, J. 1983, ApJ, 265, 1
Akritas, M. G., & Bershady, M. A. 1996, ApJ, 470, 706
Bell, E. F., Baugh, C. M., Cole, S., Frenk, C. S., & Lacey, C. G. 2003a, MNRAS, 343, 367
Bell, E. F., & de Jong, R. S. 2001, ApJ, 550, 212
Bell, E. F., McIntosh, D. H., Katz, N., & Weinberg, M. D. 2003b, ApJS, 149, 289
Bernstein, G. M., Guhathakurta, P., Raychaudhury, S., Giovanelli, R., Haynes, M. P., Herter, T., &, Vogt, N. P. 1994, AJ, 107, 1962
Bryan, G. L., & Norman, M. L. 1998, ApJ, 495, 80
Buchalter, A., Jimenez, R., & Kamionkowski, M. 2001, MNRAS, 322, 43
Bullock, J. S., Dekel, A., Kolatt, T. S., Kravtsov, A. V., Klypin, A. A., Porciani, C., & Primack, J. R. 2001a, ApJ, 555, 240
Bullock, J. S., Kolatt, T. S., Sigad, Y., Somerville, R. S., Kravtsov, A. V., Klypin, A. A., Primack, J. R., & Dekel, A. 2001b, MNRAS, 321, 559
Byun, Y.-I. 1992, Ph.D. thesis, Australian National Univ.
Catinella, B., Giovanelli, R., & Haynes, M. P. 2006, ApJ, 640, 751
Courteau, S. 1996, ApJS, 103, 363
———. 1997, AJ, 114, 2402 (C97)
Courteau, S., Andersen, D. R., Bershady, M. A., MacArthur, L. A., & Rix, H.-W. 2003, ApJ, 594, 208
Courteau, S., & Rix, H. 1999, ApJ, 513, 561 (CR99)
Courteau, S., Strauss, M. A., & Willick, J. A. 2000a, ASP Conf. Vol. 201, Cosmic Flows 1999: Towards an Understanding of Large Scale Structure (San Francisco: ASP)
Courteau, S., Willick, J. A., Strauss, M. A., Schlegel, D., & Postman, M. 2000b, ApJ, 544, 636
Dalcanton, J. J., Spergel, D. N., & Summers, F. J. 1997, ApJ, 482, 659
Dale, D. A., Giovanelli, R., Haynes, M. P., Campusano, L. E., & Hardy, E. 1999, AJ, 118, 1489
de Jong, R. S., & Lacey, C. 2000, ApJ, 545, 781 (dJL00)
De Rijcke, S., et al. 2007, ApJ, 659, 1172
de Vaucouleurs, G., de Vaucouleurs, A., Corwin, H. G., Buta, R. J., Paturel, G., & Fouque, P. 1991, Third Reference Catalog of Bright Galaxies (New York: Springer)
Dutton, A. A., van den Bosch, F. C., Dekel, A., & Courteau, S. 2007, ApJ, 654, 27 (D07)
Eke, V. R., Navarro, J. F., & Frenk, C. S. 1998, ApJ, 503, 569
Fall, S. M., & Efstathiou, G. 1980, MNRAS, 193, 189
Firmani, C., & Avila-Reese, V. 2000, MNRAS, 315, 457 (FAR00)
Geha, M., Blanton, M. R., Masjedi, M., & West, A. A. 2006, ApJ, 653, 240
Giovanelli, R., Haynes, M. P., Herter, T., Vogt, N. P., da Costa, L. N., Freudling, W., Salzer, J. J., & Wegner, G. 1997, AJ, 113, 53 (G97)
Giraud, E. 1986, ApJ, 309, 512
Gnedin, O. Y., et al. 2006, ApJ, in press (astro-ph/0607394)
Governato, F., Willman, B., Mayer, L., Brooks, A., Stinson, G., Valenzuela, O., Wadsley, J., & Quinn, T. 2007, MNRAS, 374, 1479
Graham, A. W. 2002, MNRAS, 334, 721
Gunn, J. E., & Gott, J. R. I. 1972, ApJ, 176, 1
Gurovich, S. 2007, Ph.D. thesis, Australia National University
Haynes, M. P., & Giovanelli, R. 1984, AJ, 89, 758
Heavens, A. F., & Jimenez, R. 1999, MNRAS, 305, 770
Hewett, P., et al. 2006, MNRAS, 367, 454
Jansen, R. A., Franx, M., Fabricant, D., & Caldwell, N. 2000, ApJS, 126, 271
Kannappan, S. J. 2004, ApJ, 611, L89
Kannappan, S. J., Fabricant, D. G., & Franx, M. 2002, AJ, 123, 2358 (KFF02)
Kauffmann, G., et al. 2003, MNRAS, 341, 54
Kogut, A., et al. 1993, ApJ, 419, 1
Kudrya, Y. N., Karachentseva, V. E., Karachentsev, I. D., Mitronova, S. N., Jarrett, T. H., & Huchtmeier, W. K. 2003, A&A, 407, 889
MacArthur, L. A., Courteau, S., Bell, E., & Holtzman, J. A. 2004, ApJS, 152, 175
MacArthur, L. A., Courteau, S., & Holtzman, J. A. 2003, ApJ, 582, 689 (MCH03)
Masters, K. L., Springob, C. M., Haynes, M. P., & Giovanelli, R. 2006, ApJ, 653, 861
Mathewson, D. S., Ford, V. L., & Buchhorn, M. 1992, ApJS, 81, 413
McGaugh, S. S. 2005, ApJ, 632, 859
McGaugh, S. S., & de Blok, W. J. G. 1997, ApJ, 481, 689
McGaugh, S. S., Schombert, J. M., Bothun, G. D., & de Blok, W. J. G. 2000, ApJ, 533, L99
McIntosh, D. H., Bell, E. F., Weinberg, M. D., & Katz, N. 2006, MNRAS, 373, 1321
Mo, H. J., Mao, S., & White, S. D. M. 1998, MNRAS, 295, 319 (MMW98)
Navarro, J. F., & Steinmetz, M. 2000, ApJ, 538, 477 (NS00)
Navarro, J. F., & White, S. D. M. 1994, MNRAS, 267, 401
Pierce, M. J., & Tully, R. B. 1988, ApJ, 330, 579
Pizagno, J., et al. 2007, AJ, 134, 945 (P07)
Poggianti, B. M. 1997, A&AS, 122, 399
Portinari, L., Sommer-Larsen, J., & Tantalo, R. 2004, MNRAS, 347, 691
Rhee, M.-H. 1996, Ph.D. thesis, Kapteyn Institute
Roberts, M. S. 1978, AJ, 83, 1026
Roberts, M. S., & Haynes, M. P. 1994, ARA&A, 32, 115
Rubin, V. C., Burstein, D., Ford, W. K., & Thonnard, N. 1985, ApJ, 289, 81
Sakai, S., et al. 2000, ApJ, 529, 698
Salpeter, E. E., & Hoffman, G. L. 1996, ApJ, 465, 595
Salucci, P., Frenk, C. S., & Persic, M. 1993, MNRAS, 262, 392
Sargent, W. L. W., Schechter, P. L., Boksenberg, A., & Shortridge, K. 1977, ApJ, 212, 326
Schlegel, D. J., Finkbeiner, D. P., & Davis, M. 1998, ApJ, 500, 525
Shen, S., Mo, H. J., & Shu, C. 2002, MNRAS, 331, 259
Shen, S., et al. 2003, MNRAS, 343, 978 (Sh03)
Skrutskie, M. F., et al. 2006, AJ, 131, 1163
Sprayberry, D., Bernstein, G. M., Impey, C. D., & Bothun, G. D. 1995, ApJ, 438, 72
Strauss, M. A., & Willick, J. A. 1995, Phys. Rep., 261, 271
Syer, D., Mao, S., & Mo, H. J. 1999, MNRAS, 305, 357
Tully, R. B., & Fisher, J. R. 1977, A&A, 54, 661
Tully, R. B., & Pierce, M. J. 2000, ApJ, 533, 744
Tully, R. B., Pierce, M. J., Huang, J.-S., Saunders, W., Verheijen, M. A. W., & Witchalls, P. L. 1998, AJ, 115, 2264
Tully, R. B., Verheijen, M. A. W., Pierce, M. J., Huang, J., & Wainscoat, R. J. 1996, AJ, 112, 2471
van den Bosch, F. C. 1998, ApJ, 507, 601
———. 2000, ApJ, 530, 177
———. 2002, MNRAS, 332, 456
van den Bosch, F. C., Abel, T., Croft, R. A. C., Hernquist, L., & White, S. D. M. 2002, ApJ, 576, 21
Verheijen, M. A. W. 2001, ApJ, 563, 694 (V01)
Willick, J. A. 1999, ApJ, 516, 47
Willick, J. A., Courteau, S., Faber, S. M., Burstein, D., Dekel, A., & Kolatt, T. 1996, ApJ, 457, 460
Willick, J. A., Courteau, S., Faber, S. M., Burstein, D., Dekel, A., & Strauss, M. A. 1997, ApJS, 109, 333
York, D. G., et al. 2000, AJ, 120, 1579
Zavala, J., Avila-Reese, V., Hernández-Toledo, H., & Firmani, C. 2003, A&A, 412, 633
Zwaan, M. A., van der Hulst, J. M., de Blok, W. J. G., & McGaugh, S. S. 1995, MNRAS, 273, L35